INORGANIC CHEMISTRY
FRONTIERS

RESEARCH ARTICLE

View Article Online
View Journal

Cite this: DOI: 10.1039/d6qi00862c

Dual-action peptide shuttles prevent Cu-amyloid-β-induced neurotoxicity and relocate Cu intracellularly

Michael Okafor,*[a,b] David Schmitt,[a,b] Enrico Falcone,[c] Stéphane Gasman,[a] Laurent Raibaut,[b] Christelle Hureau,*[c] Peter Faller[b] and Nicolas Vitale*[a]

Alzheimer's disease (AD) remains the most prevalent neurodegenerative disease characterized by intracellular neurofibrillary tangles of Tau protein and extracellular senile plaques built on amyloid-β (Aβ) peptides. The latter result from an abnormal processing of Amyloid Precursor Protein (APP), leading to its accumulation in plaques. *Ex vivo* analyses of AD patients' brains show an abnormally elevated concentration of metals including Cu, Zn and Fe within these plaques. Altered Cu levels have also been reported in brain regions most affected in AD. These modifications are often accompanied by reduced neuronal Cu levels and by an increased pool of extracellular labile Cu, which in turn promotes reactive oxygen species (ROS) formation. To counteract this Cu dyshomeostasis and limit Cu–Aβ-induced extracellular ROS generation, we designed and synthesized two Cu(II)-selective peptide shuttles based on kinetically optimized ATCUN sequences for fast Cu(II) extraction out of Aβ: DapHH-αR5W4^{NBD} and HDapH-αR5W4^{NBD}. They were also equipped with a fluorophore that showed a very strong response to Cu(II)-binding and release. Interestingly, these two Cu(II) shuttles displayed a dual mode of action. They promptly retrieve Cu from extracellular Aβ, stop the associated ROS formation, and hence protect both cell culture models and organotypic hippocampal slices (OHSCs) from Cu(Aβ)-induced neurotoxicity. Moreover, these shuttles import and redistribute bioavailable Cu inside cells with sequence-dependent kinetics.

Received 23rd April 2026,
Accepted 1st May 2026

DOI: 10.1039/d6qi00862c

rsc.li/frontiers-inorganic

Introduction

Copper (Cu) is an essential element that must be tightly regulated and correctly distributed within living organisms to sustain a large number of biological mechanisms.[1–3] Disturbance in its distribution can cause severe disorders including Menkes disease and Wilson's disease as well as neurodegenerative disorders such as Alzheimer's disease (AD).[1,4,5] The loss of Cu homeostasis can lead to dysregulation of normal cuproprotein functions such as antioxidant defense, iron (Fe) homeostasis or mitochondrial energy conversion.[2] In AD patients, there is an increase in blood non-ceruloplasmin bound Cu.[6–10] Interestingly, a 3–4 fold higher risk of AD has been associated with the presence of excess Cu in the blood.[10] Additionally, patients with the highest concentrations of Cu not bound to ceruloplasmin perform worse in neuropsychological tests.[10] Equally, results of various quantitative approaches carried out in several groups have shown a general decrease in brain Cu levels in AD patients.[6,7] Similarly, recent studies have shown a decrease in Cu levels in the cytoplasm of brain cells, which is associated with a 25% increase in exchangeable Cu.[11,12]

An aberrant decrease in Cu in a biological compartment often leads to loss of function of cuproproteins. Similarly, an increase in Cu concentration in a compartment most likely leads to the binding of Cu to inappropriate sites on proteins/ligands, potentially inducing a toxic gain of function. As such, the increase in extracellular labile Cu favors its binding to Aβ peptides, driving toxicity in AD.[11–14] The resulting Cu(Aβ) complex catalyzes the aerobic formation of reactive oxygen species (ROS) in the presence of a physiological reductant (*e.g.*, ascorbate, AscH$^-$) by cycling between Cu(I) and Cu(II).[15–17] This reaction is possible because the Aβ peptide forms a complex with both Cu(II) (dissociation constant, $K_d \approx 10^{-9}$–10^{-10} M) and Cu(I) ($K_d \approx 10^{-7}$–10^{-10} M) at neutral pH,[18] following a highly intricate redox mechanism.[19] Cu(Aβ) complexes have therefore been proposed to contribute to the oxidative stress described in AD.[20] This stress takes various forms, ranging from peroxidation of cell membranes to oxidation of DNA and mitochondria.[17,21]

[a]*Centre National de la Recherche Scientifique, Université de Strasbourg, Institut des Neurosciences Cellulaires et Intégratives, F-67000 Strasbourg, France. E-mail: michael.okafor@uu.se, vitalen@unistra.fr*
[b]*Biometals and Biological Chemistry, Institut de Chimie (UMR 7177), Université de Strasbourg-CNRS, 4 rue Blaise Pascal, 67000 Strasbourg, France*
[c]*Univ Toulouse, CNRS, LCC, Toulouse, France. E-mail: christelle.hureau@lcc-toulouse.fr*

ROS can also generate oxidatively modified $A\beta_{1-40/42}$ peptides, which is linked to a modified aggregation propensity or an increased resistance to proteolytic degradation.[22,23]

Cu disbalance thus seems to play an important role in AD progression, and restoring its homeostasis might be important for disease remediation. Therefore, in complement to chelating this excess extracellular Cu, it is of interest to redistribute Cu inside neuronal cells where it is missing, in a "one stone, two birds" approach. This drove the design of ionophores that act as transmembrane transporters to shuttle metal ions, such as Clioquinol (iodochlorhydroxyquin, CQ) and its derivative, PBT2, as well as GTSM (glyoxal-bis(4-methyl-thiosemicarbazonato)).[24–27] These molecules chelate Cu(II) and Zn(II) to form complexes capable of crossing cell membranes. They have shown a convincing reduction in metal-modulated Aβ aggregation *in vitro*, accompanied by improved performances in various cognitive tests in AD murine models.[27,28] CQ reached phase II clinical trials, showing improvement in various cognitive tests in advanced AD patients,[29] but negative side effects with prolonged treatment halted further development.[30,31] PBT2 developed later as a safer CQ analog was proved ineffective in phase II clinical trials.[32] Therefore, Cu(II)-selective ionophores with appropriate Cu(II) affinity and selectivity in the context of AD remain to be developed. Importantly, many available Cu(II) ionophores such as GTSM, Clioquinol or PBT2 exhibit appropriate Cu(II) affinities but suffer from poor selectivity under biological conditions.[24,33,34]

The recently developed AKH-αR5W4^{NBD} shuttle has been shown to import bioavailable Cu into cells.[35] The Cu(II)-selective binding domain of this shuttle is an amino terminal Cu(II)- and Ni(II)-binding (ATCUN) motif, a tripeptide motif with a His residue in the third position (H_2N-XxxZzzHis). ATCUN motifs are known to be very selective for Cu(II) ($K_d \approx 10^{-13}$–10^{-15} M) *versus* Zn(II), with the latter being far more abundant than Cu(II) in the brain, thus making this scaffold very appropriate for selective Cu(II) targeting.[18,36,37] αR5W4, a Cell Penetrating Peptide (CPP) optimized for efficient membrane penetration,[38] was chosen as an agent to allow cell delivery of Cu. Additional studies indicated that AKH-αR5W4^{RhodB} internalization in HeLa and PC12 cells proceeds *via* ATP-dependent endocytosis pathways, such as clathrin-mediated endocytosis and caveolin-mediated endocytosis or micropinocytosis, therefore preventing intracellular oversaturation.[39] However, this shuttle lacked the kinetics to quickly retrieve Cu from Aβ, thus hampering its effectiveness and neuroprotective potential. In this work, the ATCUN motif of AKH-αR5W4^{NBD} was kinetically optimized for the ability to accelerate Cu(II) retrieval from Aβ and suppress Cu(Aβ)-induced ROS production.

Materials and methods

Materials

All compounds used during this study were purchased from accredited merchants including sodium L-ascorbate (Sigma, A4034), DMEM/F-12 (Gibco, 11320033), Dulbecco's modified Eagle's medium – high glucose (Sigma, D5796), MEM (Thermo Fisher, 12360038), horse serum (Gibco, 26050070), fetal calf serum (Gibco, 10270-160), penicillin/streptomycin (Sigma, P4458), trypsin (Gibco, 25300-054), MTT (Fisher Scientific, 10133722), anti-giantin antibodies (Abcam, ab24586), monoclonal anti-ATP7A antibodies (Abcam, ab13995), rabbit anti-mouse Alexa Fluor 555 (Invitrogen, A-21427), donkey anti-chicken Alexa Fluor 488 (Invitrogen, A78948), recombinant mouse anti-Iba1 (Abcam, ab283319), monoclonal rabbit anti-CD68 (Abcam, ab125212) and Hoechst (Thermo Fisher, 62249).

Shuttle synthesis and purification

Peptide synthesis was carried out according to a general SPPS protocol.[35] In short, peptide synthesis was performed using Biotage® Initiator + Alstra™. Fmoc-Rink-Amide Tenta XV RAM resin (loading 0.24 mmol g^{-1}) was used. 0.5 M 1 : 1 ethyl cyano (hydroxyimino)acetate (oxime)/diisopropylcarbodiimide (DIC) was used for activation, and 2 M DIEA dissolved in *N*-methyl-2-pyrrolidone (NMP) was used as the base. 5 M acetic anhydride was used to cap unreacted free amino groups. The reaction time was 2 × 30 min coupling at ambient temperature and 2 × 5 min coupling using microwaves (μWF) at 75 °C with the exception of basic amino acids that were coupled for 2 × 30 min. Fmoc deprotection was carried out using μWF at 75 °C. Dap (2,3-diaminopropionic acid) was added as the *N*ε-allyloxycarbonyl-protected (Fmoc–Dap (Alloc)–OH) form to allow specific side chain deprotection in order to graft the fluorophore NBD. The Alloc protecting group of the Dap side chain is deprotected using tetrakis(triphenylphosphine)palladium(0), which is a palladium-based mechanism.[40] The NBD fluorophore is added to the free lysine by nucleophilic substitution of 4 eq. of NBD–Cl in the presence of DIEA. Finally, deprotection was carried out using TFA in the presence of scavengers (H_2O and triisopropylsilane). Purification was performed using reversed-phase HPLC (Hitachi Primaide equipped with a XBridge C18 BEH column, 300 Å, 5 μm, 4.6 × 150 mm, 37 °C), and the purity and mass were analysed by LC-MS (LTQ-XL Thermo Fisher).

Aβ monomer preparation

$A\beta_{1-40/42}$ peptides (DAEFRHDSGYEVHHQKLVFFAEDVGSNKGAIIGLMVGGVV-IA) were purchased from GeneCust (Dudelange, Luxembourg) with a purity grade >95%. Three different batches were obtained for $A\beta_{1-40}$ and 1 batch for $A\beta_{1-42}$. They were solubilized in 100% HFIP (hexafluoro-2-propanol) for 1 h under sonication to give a concentration of ≈40 g L^{-1} (≈1 mM). Afterwards, 100 μL was placed in 0.5 mL Eppendorf tubes and left under a fume hood for 1 week to completely evaporate HFIP. After evaporation, the Aβ peptides formed a film that was conserved at −20 °C until usage. Before use, the Aβ film was solubilized in 20 μL DMSO, vortexed briefly, then centrifuged for 30 seconds and then re-vortexed. UV-Vis measurement was carried out by adding 0.5 μL of Aβ stock solution in 100 μL Milli-Q water (ρ = 18.2 MΩ cm^{-1}). The absorbance at 280 nm was obtained and using the molar

extinction coefficient of 1400 M^{-1} cm^{-1} for Aβ monomers,[41] the final theoretical concentration of Aβ was ≈5 mM.

Peptide shuttle titration *via* Cu

In 96-well plates, peptide shuttles were added to wells containing 100 mM HEPES to a final concentration of 4 μM. Then an eq. of Cu(II) was added in steps of 0.1 eq. The fluorescence was measured using a CLARIOstar (BMG LABTECH) plate reader at an excitation wavelength of 477 nm and using a UV-STAR® microplate, a 96-well half area microplate, at an emission wavelength of 545 nm.

Selective Cu(II) retrieval from media by peptide shuttles

In 96-well plates, 4 μM Cu(II) was added to wells containing either solutions of 100 mM HEPES or DMEM : F12 nutrient 1 : 1 and an eq. concentration of peptide or Cu(II) or Cu(II) + Mn(II), Zn(II) and Fe(III). The fluorescence was measured using a CLARIOstar (BMG LABTECH) plate reader at an excitation wavelength of 477 nm and between 490 and 600 nm emission wavelength for 2 h at an interval of 5 min using a UV-STAR® microplate, a 96-well half area microplate.

Retrieval of Cu by peptide shuttles from Aβ

The emission intensity of NBD on peptide shuttles was used as a readout. Using a Horiba Fluoromax Plus fluorimeter, in a 500 μL 1 cm path quartz cuvette, 10 μM Aβ and 5 μM AKH-αR5W4^{NBD}, DapHH-αR5W4^{NBD} or HDapH-αR5W4^{NBD} were added to a solution of 100 mM HEPES or 10% DMEM to determine the estimated 100% unsaturated emission intensity at 545 nm. The same was done for 10 μM Cu(II)–Aβ 1 : 2 and 5 μM Cu(II)-AKH-αR5W4^{NBD}, DapHH-αR5W4^{NBD} or HDapH-αR5W4^{NBD} 1 : 1 to determine the estimated 100% saturated emission level. Afterwards, 5 μM of AKH-αR5W4^{NBD}, DapHH-αR5W4^{NBD}, or HDapH-αR5W4^{NBD} was added to the mixture of 10 μM Cu(II) : Aβ 1 : 2, and the emission was recorded at 545 nm every 30 seconds for up to 2 h at 25 °C.

Release of Cu by peptide shuttles in GSH

Using a Horiba Fluoromax Plus fluorimeter, in a 500 μL 1 cm path quartz cuvette, 5 mM GSH and 5 μM AKH-αR5W4^{NBD}, DapHH-αR5W4^{NBD}, or HDapH-αR5W4^{NBD} were added to a 100 mM HEPES buffer pH 7.4. The solution was excited at 477 nm and recorded at 545 nm to determine the emission intensity of the peptide without Cu(II). The intensity of Cu(II)-AKH-αR5W4^{NBD}, DapHH-αR5W4^{NBD} or HDapH-αR5W4^{NBD} was recorded in the absence of GSH, and then 5 mM GSH was added from a stock solution at 200 mM and left to react for up to 12 h at 37 °C.

Inhibition of ascorbate oxidation by peptide shuttles

Using the CLARIOstar (BMG LABTECH) plate reader, experiments were carried out in a UV-STAR® microplate, a 96-well half area microplate. The absorbance of 100 μM $AscH^-$ (OD ≈ 1.5) was recorded at 265 nm under different conditions to indirectly measure ROS production. The final volume per well was 100 μL and was buffered at pH 7.4 using 100 mM HEPES. The initial rate of ascorbate consumption was determined by taking the first 20 min portion of the curve considered linear.

Toxicity assay on PC12 cells

PC12 cells were maintained in culture in DMEM high glucose (4500 mg mL^{-1}) with 10% horse serum, 5% FBS and 1% penicillin/streptomycin as described previously.[42] The cells were split once a week using trypsin for detachment and replaced by a fresh batch of cells after a maximum of 15 splits.

In 96-well plates, 50 000 cells were plated and incubated for 24 h. A solution of monomerized Aβ complex in 10% DMEM (diluted in a salt solution (0.2 g L^{-1} $CaCl_2$, 0.0001 g L^{-1} Fe$(NO_3)_3$, 0.098 g L^{-1} $MgSO_4$, 0.4 g L^{-1} KCl, 3.7 g L^{-1} $NaHCO_3$, 6.4 g L^{-1} NaCl, 0.11 g L^{-1} NaH_2PO_4, and 4.5 g L^{-1} D-glucose)) was prepared in microcentrifuge tubes, with/without the addition of AKH-αR5W4^{NBD}, DapHH-αR5W4^{NBD} or HDapH-αR5W4^{NBD} for 10 min or 1 h. Afterwards, 500 μM $AscH^-$ was added to the tubes and vortexed, and the mixture was then added to PC12 cells. After 24 h, the cell medium was replaced with 200 μL of pure DMEM containing 10% of 5 mg mL^{-1} MTT solution and incubated for 4 h at 37 °C. After a 4 h incubation at 37 °C, the medium was replaced with 150 μL DMSO and agitated for 5 min at room temperature. In new 96-well plates, 50 μL solution of each well was diluted with 150 μL of pure DMSO solution. Lastly, the absorbance was read at 595 nm. Each condition corresponds to the average of three recordings on the same plate and each experiment was replicated independently three times.

ATP7A delocalization assay

Glass coverslips were treated with poly-L-lysine for 15 min in 4-well NUNC plates. Afterwards, the coverslips were rinsed with enriched DMEM. PC12 cells were then cultured at a density of 1 × 10^5 cells per well, 24 h before experiments. In 10% DMEM solution, EDTA, GTSM or Cu shuttles were added alone or precomplexed to Cu(II). This mixture was added to the cells and incubated for 1 h. After the experiment, the medium was removed, and the cells were fixed with 4% PFA (paraformaldehyde), and then permeabilized and saturated in 0.2% Triton X-100 and 1× PBS containing 10% DS (donkey serum) at 37 °C. The cells were then incubated overnight at 4 °C with chicken anti-ATP7A 1/5000 and rabbit anti-mouse Giantin 1/500 in 3% BSA (bovine serum albumin). The next day the cells were washed 3 times with PBS and then incubated with donkey anti-chicken AlexaFluor 488 and anti-rabbit AlexaFluor 555 secondary antibodies and Hoechst at 1/1000 dilution for 45 min at 37 °C before being rinsed and mounted in Mowiol.

Organotypic hippocampal slice culture (OHSC)

The procedure recapitulates that of Stoppini *et al.* 1991 with minor modifications.[43] CD1 mice between ages P6 and P10 were used for OHSC. The dissection media consist of cold Hanks balanced salt solution (HBSS) and the slice culture media consist of 50% MEM solution, 25% HBSS, 25% horse serum inactivated, 1% streptomycin–penicillin, 25 mM HEPES and 2 mM L-glutamine. D-Glucose was added to the cell culture

solution for a final concentration of 4.5 g L^{-1} (the culture media should be at pH 7.2).

Mice were decapitated and placed immediately in a 25 mL beaker containing ice cold HBSS. Using scissors, the skull was cut through and the brain extracted, and then transferred to a 30 mm Petri dish filled with cold HBSS. The hippocampus was extracted by holding down one hemisphere with forceps and separating the other with a spatula. Both hippocampi were extracted and placed on the Mcllwain tissue chopper board perpendicular to the blade, with the micrometer set at 400 μm and the blade wetted with cold HBSS before chopping. After brain slices were ready, the slices were transferred to a 30 mm Petri dish filled with cold HBSS, and each slice was separated using 2 spatulas. Each slice containing the dentate gyrus, CA1, and CA3 regions was placed on the Millicell inserts with 6 hippocampal slices per well of a 6-well plate. The plate was placed in an incubator and the media were changed every 2–3 days. The slices were kept in culture for two weeks to acclimatize to their new environment before the experiment.

Cu toxicity rescue experiment in OHSCs

After two weeks of culture, hippocampal slices were treated with different conditions for 48 h in DMEM solution containing 25 mM HEPES. Prior to the experiment, preparation of Aβ monomers for monomeric conditions was carried out (see SI Materials and methods).

The Cu(II)Aβ complex was synthesized by mixing 0.5 eq. of Cu (10 μM) with 1 eq. of Aβ (20 μM). After complexation of Cu (Aβ), DapHH-αR5W4^{NBD} or HDapH-αR5W4^{NBD} was added or not at 0.5 eq. and vortexed. The solution was immediately placed on top of the slices (the time solution will drain into the well out of the Millicell insert). Slices were left for 48 h at 37 °C.

PI staining

A salt solution (0.2 g L^{-1} $CaCl_2$, 0.0001 g L^{-1} $Fe(NO_3)_3$, 0.098 g L^{-1} $MgSO_4$, 0.4 g L^{-1} KCl, 3.7 g L^{-1} $NaHCO_3$, 6.4 g L^{-1} NaCl, 0.11 g L^{-1} NaH_2PO_4, and 4.5 g L^{-1} D-glucose) containing 5 μM PI and 25 mM HEPES was prepared, and 100 μL was placed in each well on top of every slice and incubated for 1 h at 37 °C. Afterwards, the slices were fixed with 4% PFA for 40 min. From each condition, 3 slices were cut out of the Millicell insert after fixation and treated with Hoechst for 30 min and then mounted on slides. Slides were left at room temperature to semi-dry for 1 h and then images were acquired at 405 nm and 555 nm using a fluorescence microscope, ZEISS Axio Imager M2, coupled with a motorized board for mosaic imaging.

Immunohistochemistry

The remaining 3 slices were cut out of the Millicell insert and were washed with PBS. The slices were permeabilized and non-specific sites were blocked with PBS solution containing 0.3% Triton and 10% goat serum for 3 hours under agitation. Afterwards, the slices were rinsed once with PBS and then incubated in PBS containing 1 mg ml^{-1} BSA (bovine serum albumin) overnight at 4 °C with primary antibodies (mouse anti-Iba1 1 : 100 and rabbit anti-CD68 1 : 1000). The slices were washed 3 times with PBS for 5 min each with gentle shaking and then incubated with secondary anti-mouse 555 nm and anti-rabbit 647 nm antibodies at 1 : 1000 dilution in PBS containing 1 mg mL^{-1} BSA for 3 hours at room temperature with gentle shaking. Finally, the slices were washed 3 times with PBS for 5 min each with gentle shaking and mounted on glass slides by placing the slices with the membrane side flat on the slides. Mowiol was added on each slice followed by the cover. The slides were left to dry at room temperature in obscurity for at least 24 h before confocal imaging using Leica SP5.

Analysis of cell viability in OHSCs

Cell viability measurements were performed by counting the total cell number *via* nucleus staining with Hoechst using the QuPath software. Cells were also incubated with propidium iodine (PI), and the mean fluorescence intensity of the PI staining was calculated for each cell nucleus. Cells with PI staining above a threshold were deemed PI positive and divided by the total number of cells (Hoechst positive) to calculate the percentage of Hoechst + PI + cells.

Analysis of microglial activation in OHSCs

Microglial activation analysis was carried out by labelling cells positive for both Iba1 and CD68. Iba1 cells were counted using QuPath software and labelled as microglial cells. From cells positive for Iba1, the average number of microglial cells with a threshold of CD68 staining was labelled as activated microglial cells. The percentage of activated microglial cells is expressed as CD68 positive cells divided by Iba1 positive cells. All data were normalized with respect to the control group.

Statistical analysis

All analyses were carried out using GraphPad Prism 9.3.1. Datasets were subjected to the Shapiro test for normality. For comparisons of the mean, a parametric test with Tukey's multiple comparison post-test or a non-parametric Kruskal–Wallis test with Dunn's multiple comparison test was carried out.

Results

In the quest for efficient peptide shuttles in regard to the arrest of ROS production, the rate of Cu(II) removal from Cu (Aβ) complexes was identified as an additional key parameter.[35] Based on a large series of kinetic investigations, the presence of two His, either at positions 1 and 3 (H_2N-HisXxxHis) or positions 2 and 3 (H_2N-XxxHisHis), was shown to allow the ATCUN scaffold to overcome such kinetic limitations.[44,45] Therefore, we designed, synthesized and probed two different ATCUN motifs. These two shuttles, H_2N-Dap-His-His-αR5W4^{NBD} (DapHH-αR5W4^{NBD}) and H_2N-His-Dap-His-αR5W4^{NBD} (HDapH-αR5W4^{NBD}), were functionalized with a nitrobenzodiazole (NBD) fluorophore on the Dap (2,3-diaminopropionic acid, a lysine analogue with a shorter side chain) residue inside the ATCUN motif for closer proximity to the bound Cu(II) (see Methods and Fig. S1A–C).

These novel shuttles were compared to the H_2N-Ala-Lys-His-αR5W4^{NBD} (AKH-αR5W4^{NBD}, Fig. 1).

Physico-chemical characterization of Cu(II) peptide shuttles

The differences in the physico-chemical properties of the Cu(II)-selective peptide shuttles (DapHH-αR5W4^{NBD} and HDapH-αR5W4^{NBD}) in comparison with the parent molecule, AKH-αR5W4^{NBD}, were investigated (Fig. 1A, S1A–E). The UV-Vis spectra displayed similar absorption bands at 350 and 490 nm due to the NBD chromophore (Fig. S1D). A red-shift was observed for the Cu(II)-HDapH-αR5W4^{NBD} complex (Fig. S1D and S1E, red traces), suggesting a structural change upon Cu(II) binding. The emission of both DapHH-αR5W4^{NBD} and HDapH-αR5W4^{NBD} was then studied by fluorimetry. Since the NBD fluorophore has an excitation maximum at 480 nm and an emission maximum at 545 nm in aqueous medium, the two peptides were excited at 477 nm and the fluorescence emission spectra were recorded between 490 nm and 600 nm. The emission maximum was observed at 545 nm and the successive additions of Cu(II) in a 0.1 equivalent step led to a linear decrease in emission intensity at 545 nm up to 1 equivalent (Fig. S2A). For both DapHH-αR5W4^{NBD} and HDapH-αR5W4^{NBD}, 98% quenching of NBD emission was recorded, thus validating the intended design of the peptides to display a high percentage of fluorescence quenching upon Cu(II) binding.

Next, we investigated the capacity of the shuttles to withdraw Cu(II) from cell culture media such as DMEM 10% (DMEM diluted in salt solution) and DMEM/F12 (D/F). For this, we spiked DMEM 10% media or D/F media with 5 μM Cu(II) for one minute, then added AKH-αR5W4^{NBD}, DapHH-αR5W4^{NBD} or HDapH-αR5W4^{NBD} and then recorded the NBD emission for 5 h in a plate reader. Controls were carried out simultaneously in the absence of Cu and with the shuttles pre-complexed with Cu(II) before addition to the media, allowing the estimation of NBD emission in both the 0% saturated state and the 100% saturated state, respectively (Fig. 1B, S2B–E). Both DapHH-αR5W4^{NBD} and HDapH-αR5W4^{NBD} out-performed AKH-αR5W4^{NBD} in terms of the rate of withdrawing Cu(II) from the cell culture media (Fig. 1B). Indeed, all three peptide shuttles were capable of withdrawing Cu(II) from DMEM 10% media, with the rate following the trend: HDapH-αR5W4^{NBD} > DapHH-αR5W4^{NBD} > AKH-αR5W4^{NBD} (Fig. S2B &

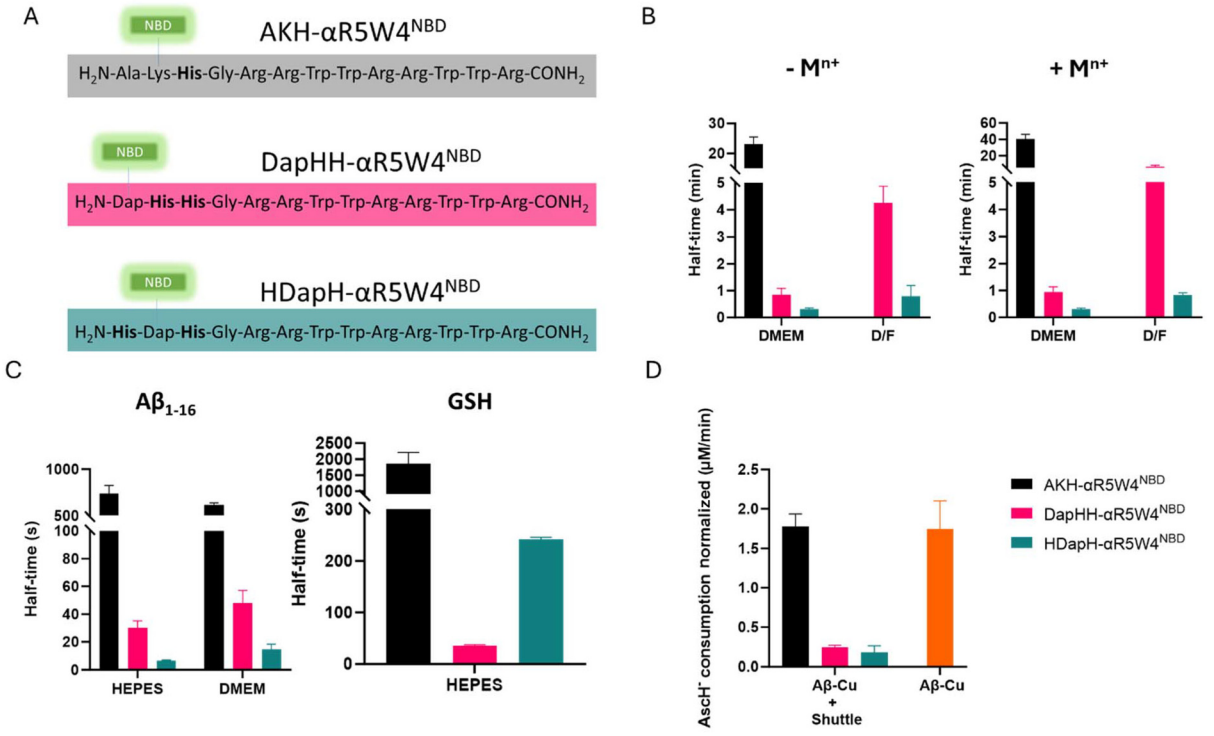

Fig. 1 Properties of DapHH-αR5W4^{NBD} and HDapH-αR5W4^{NBD} shuttles. (A) Amino acid sequence of the peptide shuttles under study: AKH-αR5W4^{NBD}, DapHH-αR5W4^{NBD} and HDapH-αR5W4^{NBD}. (B) Half-time of the selective withdrawal of Cu(II) by the shuttles in cell culture media containing Cu(II) alone or in addition to M^{n+} (Fe(III), Zn(II) and Mn(II)). AKH-αR5W4^{NBD} Cu(II) withdrawal was too slow in D/F media; data not shown. Conditions: Cu(II) = AKH-αR5W4^{NBD} = DapHH-αR5W4^{NBD} = HDapH-αR5W4^{NBD} = 5 μM, DMEM 10%, D/F 100%, 25 °C, n = 3. (C) Retrieval of Cu(II) from Aβ_{1-16} by the shuttles in HEPES or DMEM 10% media and reduction/release of Cu(II) by GSH in HEPES. Conditions: AKH-αR5W4^{NBD} = DapHH-αR5W4^{NBD} = HDapH-αR5W4^{NBD} = 5 μM; Aβ_{1-16} = 10 μM; Cu(II) = 5 μM, HEPES 100 mM pH 7.4, 25 °C, n = 3. (D) Inhibition of $AscH^-$ consumption by the shuttles monitored by the absorbance of $AscH^-$ at 265 nm (see Fig. S2E for the complete kinetic curves). Addition of $AscH^-$ was carried out at t_0 and Cu(II)Aβ_{1-16} at 5 min and addition of the shuttles at 10 min. The graph shows the initial consumption of $AscH^-$ in the first 20 min after the addition of the shuttles in the presence of Cu(II)Aβ_{1-16}, normalized with values from samples in the absence of Cu(II)Aβ_{1-16}. Conditions: $AscH^-$ = 100 μM, 5 μM Cu(II)DapHH-αR5W4^{NBD} or Cu(II)HDapH-αR5W4^{NBD}, Aβ_{1-16} = 10 μM, Cu(II) = DapHH-αR5W4^{NBD} = HDapH-αR5W4^{NBD} = 5 μM, HEPES 100 mM pH 7.4, n = 2 independent experiments.

D). In addition, HDapH-αR5W4^{NBD} completely withdrew Cu(II) from D/F media (higher concentration of amino acids), with DapHH-αR5W4^{NBD} retrieving >80% and AKH-αR5W4^{NBD} withdrawing ≈50% over the measurement duration (Fig. 1B, S2C & E and Table S1). Altogether, these results confirm the successful design of shuttles with faster Cu(II)-retrieval kinetics.

We then validated the selectivity of DapHH-αR5W4^{NBD} and HDapH-αR5W4^{NBD} to withdraw specifically Cu(II) from cell media containing other essential d-block metal ions. For this, we spiked both DMEM 10% and D/F media with Cu(II) and M^{n+} (Fe(III), Zn(II) and Mn(II)), each at 5 μM before addition of AKH-αR5W4^{NBD}, DapHH-αR5W4^{NBD} or HDapH-αR5W4^{NBD} after a minute. No major difference was observed in the percentage or withdrawal kinetics for the three peptide shuttles in the presence or absence of other d-block metal ions in DMEM (Fig. 1B, S3A–D and Table S1). However, a slight reduction in the average kinetics of Cu withdrawal by DapHH-αR5W4^{NBD} was observed in D/F, although HDapH-αR5W4^{NBD} stayed constant. Again, HDapH-αR5W4^{NBD} was generally the fastest, followed by DapHH-αR5W4^{NBD} and then AKH-αR5W4^{NBD} (Fig. 1B).

We next compared the kinetics of selective Cu(II) withdrawal by DapHH-αR5W4^{NBD} and HDapH-αR5W4^{NBD} with that of GTSM, a prototypical Cu(II) ionophore (Fig. S4). HDapH-αR5W4^{NBD} but not DapHH-αR5W4^{NBD} displayed comparable kinetics of Cu(II) withdrawal to that of GTSM in both DMEM 10% and D/F media (half-time <1 min).

Next, we investigated the capacity of the two peptide shuttles to withdraw Cu(II) from $A\beta_{1-16}$, the domain responsible for Cu binding in Aβ peptides.[22,46] Rapid retrieval of Cu(II) from $A\beta_{1-16}$ was observed in HEPES buffer in 10% DMEM for both peptides (Fig. 1C, S5A and B), with the complete retrieval occurring in less than two minutes compared to over an hour for AKH-αR5W4^{NBD}. Among these two shuttles, HDapH-αR5W4^{NBD} acted faster than DapHH-αR5W4^{NBD} (Fig. 1C). Moreover, unlike the parent AKH-αR5W4^{NBD} peptide, both HDapH-αR5W4^{NBD} and DapHH-αR5W4^{NBD} are able to promptly retrieve most Cu(II) from $A\beta_{1-16}$ even in the presence of $A\beta_{4-16}$, a truncated Aβ peptide containing a high-affinity ATCUN motif, which is also present in the brain (Fig. S6).[47] This is likely due to the faster Cu(II) binding to the optimized HDapH and DapHH motifs compared to the canonical Xxx-Zzz-His motif found in both AKH-αR5W4^{NBD} and $A\beta_{4-16}$.

We then investigated whether physiological levels of glutathione (GSH, 5 mM) could reduce Cu(II) bound to DapHH-αR5W4^{NBD} and HDapH-αR5W4^{NBD}, given that the reduction of Cu(II) by a reducing agent like GSH renders bound Cu bioavailable. Both DapHH-αR5W4^{NBD} and HDapH-αR5W4^{NBD} displayed half-times of only a few minutes, whereas that of AKH-αR5W4^{NBD} required tens of minutes (Fig. 1C, Fig. S5C and Table S2). This is in line with previous studies that have shown the H_2N-HisXxxHis and H_2N-XxxHisHis motifs to be easily reduced in comparison with the canonic H_2N-XxxZzzHis motif.[44,45] Notably, Cu(II)-DapHH-αR5W4^{NBD} was reduced faster than Cu(II)-HDapH-αR5W4^{NBD} in HEPES buffer at pH 7.4 (Fig. 1C, Fig. S5C and Table S2).

We next tested the capacity of the shuttles to inhibit Cu(Aβ)-induced ROS production catalyzed by $AscH^-$. $AscH^-$ was monitored at 265 nm, a classical assay that mirrors ROS formation.[35] The initial rate of ROS production by Cu(II)$A\beta_{1-16}$ indirectly measured during the first 20 minutes after the addition of $AscH^-$ was 1.6 ± 0.1 μM min^{-1}, in agreement with reported values.[18] Upon addition of DapHH-αR5W4^{NBD} or HDapH-αR5W4^{NBD}, an immediate reduction in ROS production was observed (Fig. 1D and S2D and E), which was not the case for the AKH-αR5W4^{NBD} shuttle.[35]

In summary, both DapHH-αR5W4^{NBD} and HDapH-αR5W4^{NBD} have proven to be much faster than AKH-αR5W4^{NBD} in retrieving Cu(II) from $A\beta_{1-16}$ and therefore in suppressing Cu(Aβ)-induced ROS production. In the following studies, we investigated whether these shuttles are also able to transfer and release Cu intracellularly in addition to preventing cells from extracellular Cu(Aβ)-induced ROS toxicity.

Cellular characterization of DapHH-αR5W4^{NBD} and HDapH-αR5W4^{NBD} in PC12 cells

Firstly, we tested the toxicity of these shuttles on PC12 cells, a well-known neurosecretory cell model.[48] Neither DapHH-αR5W4^{NBD}, HDapH-αR5W4^{NBD} nor the corresponding Cu(II) complexes were toxic below 10 μM (Fig. S7A). This indicates that micromolar concentrations of the peptide shuttles, unlike GTSM (toxic at nanomolar concentrations (Fig. S7B)), do not lead to intracellular toxic levels of Cu. It is possible that the cell toxicity induced by GTSM results from too high levels, too fast release, and/or release of Cu in inappropriate intracellular compartments. We then investigated the cell entry of 5 μM of these Cu(II)(peptides) complexes into PC12 cells using confocal microscopy. Over a 30 min incubation period, we observed membrane binding followed by a gradual increase in intracellular fluorescence attributed to an intracellular release of Cu by the peptide shuttles (Fig. 2A and S9A). Compared to the peptide shuttle without Cu, the Cu(II)-complexed shuttles showed lower membrane and intracellular fluorescence within the first minutes of incubation, likely reflecting a delay in the Cu(II) expulsion from the Cu(II)(shuttle) complexes after internalization (Fig. 2A). The intracellular fluorescence signal mostly corresponded to vesicular structures similar to endosomes, which points to a cell entry mechanism involving endocytosis as recently established for the αR5W4 CPP.[39] Interestingly, cells incubated with Cu(II)(HDapH-αR5W4^{NBD}) displayed a more rapid increase in vesicular fluorescence compared to those incubated with Cu(II)(DapHH-αR5W4^{NBD}). This was unexpected given that *in vitro* data demonstrated that Cu(II)(DapHH-αR5W4^{NBD}) is reduced faster than Cu(II)(HDapH-αR5W4^{NBD}) at pH 7.4 (Fig. 1C, GSH). This result suggests that other factors influence the intracellular Cu release from the shuttles. For instance, we surmised that the progressive acidification along the endolysosomal pathway, the major cellular entry route used by αR5W4 CPP,[39] could be one of these factors. We hence compared the reduction kinetics of the two Cu-shuttles using GSH in 100 mM MES buffer at pH 5. In this case, in contrast to pH 7.4 (Fig. 1C and S5C) but in line with cellular experiments (Fig. 2), Cu(II)-HDapH-αR5W4^{NBD} was reduced faster than Cu(II)-DapHH-αR5W4^{NBD} (Fig. S8).

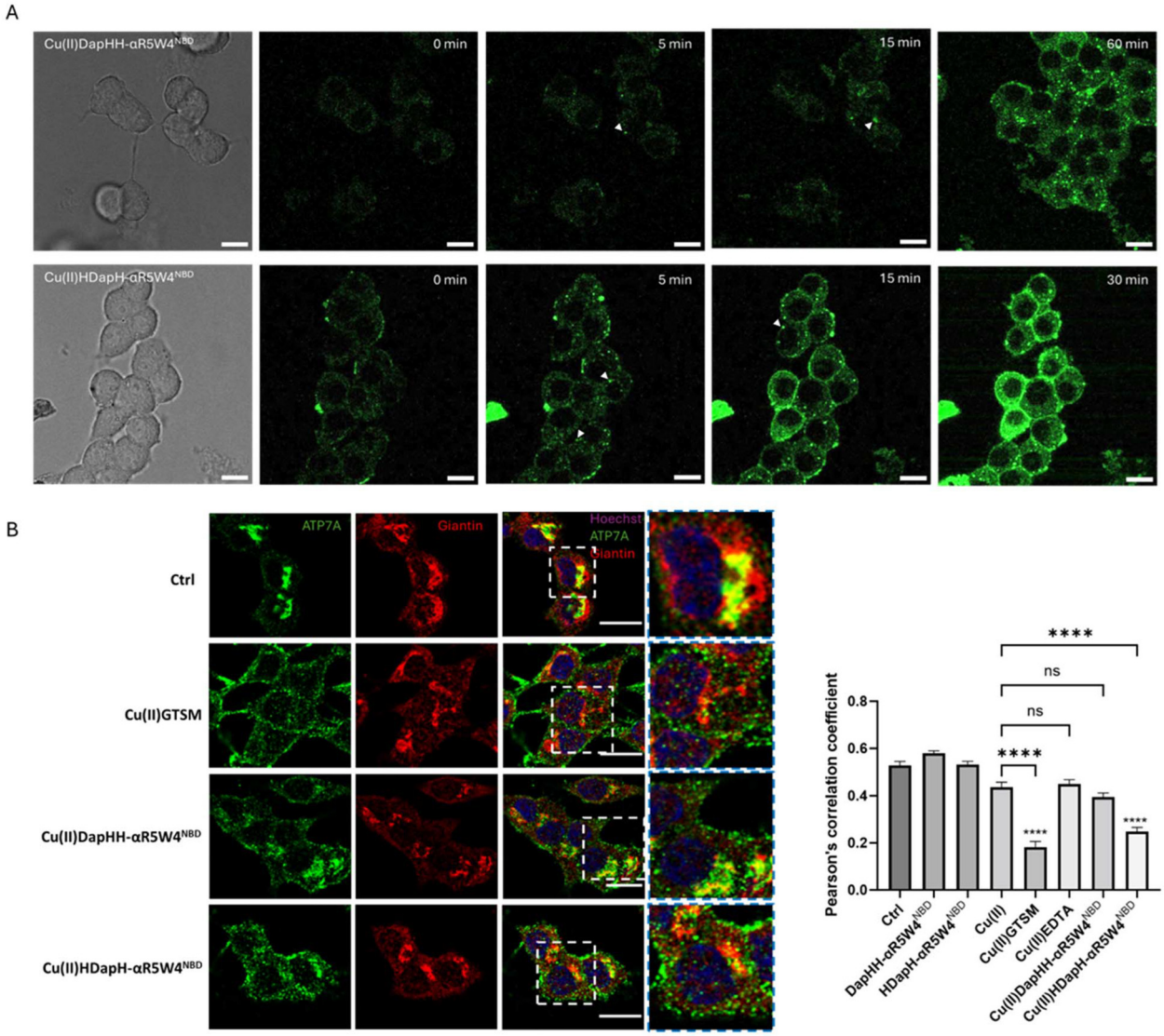

Fig. 2 Cu import by HDapH-αR5W4^{NBD} induced delocalization of ATP7A from the TGN to vesicular structures. (A) Representative images at the indicated time obtained from live imaging performed on 5 × 10^4 PC12 cells incubated with 5 μM Cu(II)(DapHH-αR5W4^{NBD}) or Cu(II)(HDapH-αR5W4^{NBD}) at 37 °C using a Leica TCS SP5 (II) confocal microscope, with an excitation wavelength at 477 nm for 30 min. White arrows illustrate internalized shuttles. Time point zero is about 1 minute after incubation with the peptide shuttles. Bars = 10 μm. (B) Quantification of the colocalization between ATP7A and Giantin (Golgi marker) staining was measured as Pearson's correlation coefficient. PC12 cells were incubated for 1 h in DMEM alone (control = Ctrl) or 5 μM Cu(II), Cu(II)-EDTA, DapHH-αR5W4^{NBD}, Cu(II)(DapHH-αR5W4^{NBD}), HDapH-αR5W4^{NBD} and Cu(II)(HDapH-αR5W4^{NBD}) or 1 μM Cu(II)-GTSM, before fixation. Blue: Hoechst (nucleus marker); green: ATP7A; red: Giantin. See Fig. S9B for images of other conditions. Representative images are shown. Bars = 10 μm. n = 3 independent experiments. A zoomed inset is displayed on the outermost right panel. Number of cells analyzed ≥27 for each condition. A parametric ordinary one-way ANOVA test was carried out with Dunnett's multiple comparison test, **** $p < 0.0001$.

Therefore, acidification along the endolysosomal pathway, as well as a myriad of other factors such as reducing agents, could be responsible for the release of Cu from these shuttles.

Having validated that Cu(II)(DapHH-αR5W4^{NBD}) and Cu(II)(HDapH-αR5W4^{NBD}) (i) can penetrate into PC12 cells, (ii) localize inside vesicular structures, and (iii) may gradually release Cu within endosomes, we then indirectly probed the bioavailability of the imported Cu by monitoring the delocalization of the Golgi-associated Cu transporter, ATP7A. This protein is known to delocalize from the perinuclear Golgi area to vesicles in proximity to the plasma membrane when the cell needs to expel Cu in excess.[49] This assay is important to differentiate between shuttles capable of importing bioavailable Cu into cells *versus* those that just increase the total Cu concentration, that might not be useable by the cell. Treatment with Cu(II)(HDapH-αR5W4^{NBD}) induced a significant delocalization of ATP7A to vesicular structures close to the plasma membrane in PC12 cells after 1 h incubation, thereby confirming the presence of cytosolic bioavailable Cu (Fig. 2B and S9B). However, Cu(II)(DapHH-αR5W4^{NBD}) only showed a tendency toward

ATP7A delocalization, which is in line with the slower increase in fluorescence signal in these cells (Fig. 2A). These observations suggest that although DapHH-αR5W4^{NBD} is internalized into the cell, it is slow to release bioavailable Cu. It is of note that the shuttles are not fixable and therefore do not contribute to the green signal of ATP7A when cells were fixed with PFA, as confirmed by controls (Fig. 2B and S9B).

Next, we investigated the ability of DapHH-αR5W4^{NBD} and HDapH-αR5W4^{NBD} to protect PC12 from Cu(II)–Aβ peptide-induced toxicity in the presence of a physiological concentration of AscH$^-$ (500 μM).[50–52] Cu(II)Aβ$_{1-16}$ was toxic only in the presence of a reductant. This toxicity was reversed in the presence of DapHH-αR5W4^{NBD} or HDapH-αR5W4^{NBD}, but not in the presence of AKH-αR5W4^{NBD} (Fig. 3A), except after pre-

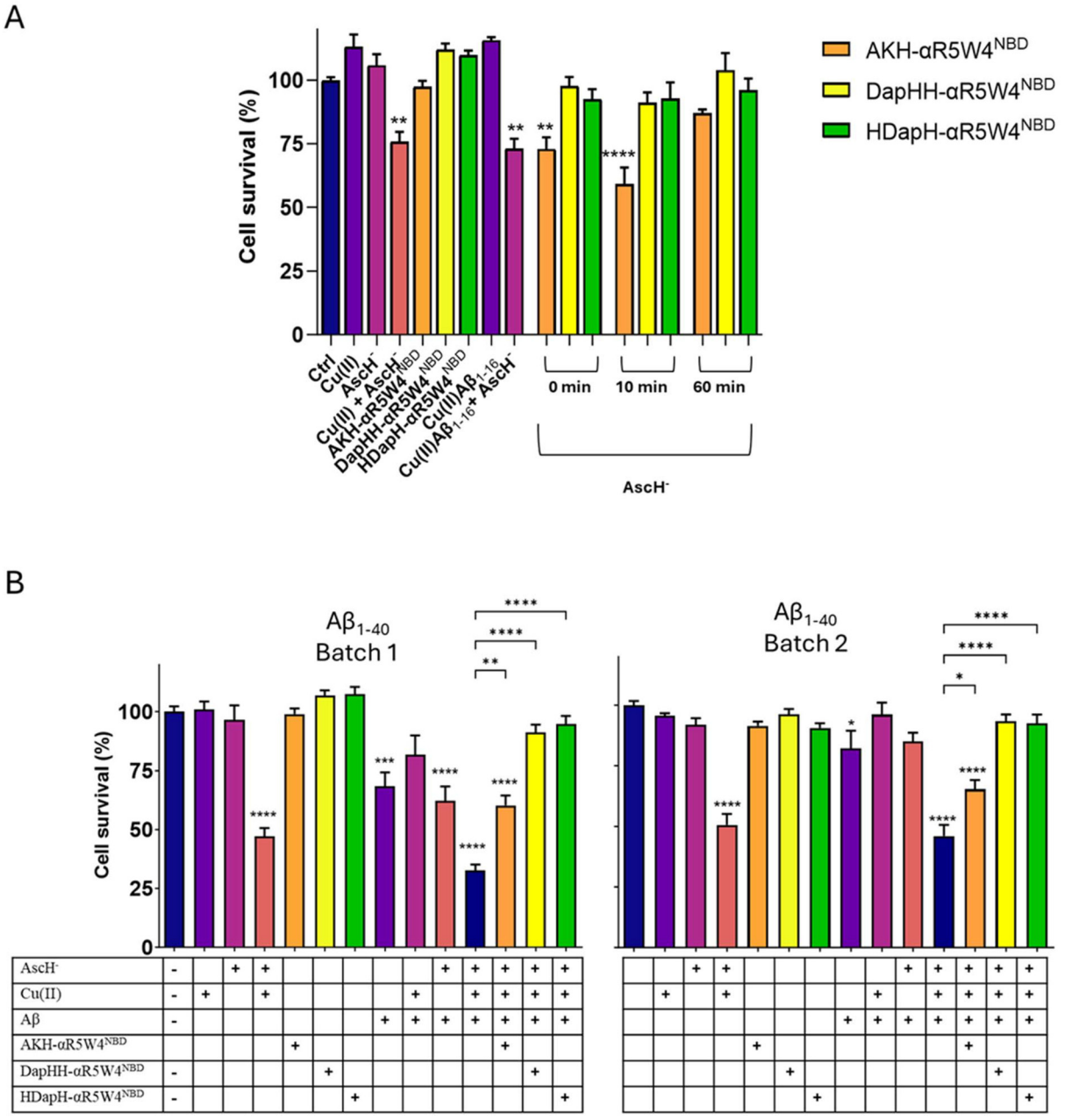

Fig. 3 DapHH-αR5W4^{NBD} and HDapH-αR5W4^{NBD} prevent Cu-induced ROS and associated toxicity in PC12 cells. (A) 5 μM AKH-αR5W4^{NBD}, DapHH-αR5W4^{NBD} or HDapH-αR5W4^{NBD} was incubated with 10 μM Cu(II)Aβ$_{1-16}$ 0.5 : 1 in 10% DMEM in a test tube for 0, 10 or 60 min before addition of 500 μM AscH$^-$ and immediate administration on the PC12 cells. Experiments were performed in triplicate, n = 3. A normality D'Agostino & Pearson test was passed. A parametric ordinary one-way ANOVA test was carried out with Tukey's post-test, * $p < 0.05$, ** $p < 0.01$, **** $p < 0.0001$. (B) PC12 cells were incubated with 5 μM AKH-αR5W4^{NBD}, DapHH-αR5W4^{NBD} or HDapH-αR5W4^{NBD} with 10 μM Cu(II)(Aβ$_{1-40}$) 0.5 : 1 and 500 μM AscH$^-$ for 24 h. Experiments were performed in triplicate, n = 3. A parametric ordinary one-way ANOVA test was carried out with Tukey's multiple comparison test, * $p < 0.05$, ** $p < 0.01$, **** $p < 0.0001$. Experiments were carried out in 10% DMEM. "+" signifies the presence of a particular molecule.

incubation of AKH-αR5W4^{NBD} with Cu(II)Aβ$_{1-16}$ for an hour. This is in line with the faster retrieval of Cu(II) from Aβ and arrest of ROS production by the DapHH-αR5W4^{NBD} and HDapH-αR5W4^{NBD} shuttles as demonstrated *in vitro* (Fig. 1C and D). The ability of these shuttles to rescue PC12 cells from Cu-induced toxicity was also studied using three independent batches of the full-length Aβ$_{1-40}$ peptide. In agreement with the known variability in Aβ-induced cell toxicity,[53] of the three batches of Aβ$_{1-40}$ tested, only batch 1 and 2 had significant toxicity on PC12 cells at 10 μM, whereas batch 3 showed only a tendency towards toxicity (Fig. 3B, Fig. S10). In the presence of Cu(II)Aβ$_{1-40}$, upon addition of AscH$^-$, there was a significant increase in toxicity for all three Aβ$_{1-40}$ batches due to Cu(Aβ)-induced ROS production, as observed for Aβ$_{1-16}$ (Fig. 3A). Importantly, DapHH-αR5W4^{NBD} and HDapH-αR5W4^{NBD} fully rescued this toxicity. In conclusion, both DapHH-αR5W4^{NBD} and HDapH-αR5W4^{NBD} are capable of preventing Cu(II)Aβ$_{1-16}$ and Cu(II)Aβ$_{1-40}$ induced toxicity in PC12 cells in the presence of AscH$^-$.

Organotypic hippocampal slice culture (OHSC) model of AD

OHSC is a relevant model to study neurodegenerative diseases and has been used to investigate Aβ toxicity,[54–57] oxidative stress remediation[58,59] and glial activation[60,61] linked to Alzheimer's disease. Its value lies in its similarity to *in vivo* animal models, particularly the preservation of neuronal connections. Therefore, after establishing the shuttles' ability to prevent ROS production, penetrate the cellular membrane and deliver bioavailable Cu in a monoculture system, we next sought to determine whether these complex functions translated to overall tissue protection in an OHSC model of extracellular Cu-driven toxicity in the context of AD.

Brain slices with a visible dentate gyrus (DG) and CA3, CA2, and CA1 regions were obtained from CD1 mice between P6 and P10 and placed in culture for 2 weeks before treatment. Hippocampal slices were incubated with Cu(II)Aβ$_{1-40}$ or Cu(II)Aβ$_{1-42}$ in the presence or absence of DapHH-αR5W4^{NBD} or HDapH-αR5W4^{NBD} for 48 h without AscH$^-$ supplementation because the brain intrinsically possesses between 0.1 and 1 mM AscH$^-$,[50,51] in contrast to cultured 2D cells.[62] Cell density was analyzed by counting the number of Hoechst-labeled nuclei, which were similar for each condition, validating slice quality and indicating low variability (Fig. 4A and B). Cell toxicity on organotypic hippocampal slices was determined by treating slices with propidium iodide (PI) for 1 h before Hoechst staining. PI-labelled cells represent cells with a compromised plasma membrane, thus permitting PI to intercalate into cell DNA. Of note, PI staining does not directly detect cell death but rather permeabilization of the plasma membrane, one of the first stages toward cell death upon ROS-induced membrane alteration.

Treatment of OHSCs with 20 μM of monomeric Aβ$_{1-40}$ or Aβ$_{1-42}$ for 48 h did not lead to detectable toxicity (Fig. 4). However, in Cu(II)-treated cells, there was a significant increase in PI-stained nuclei, suggesting that 10 μM of extracellular Cu(II) is toxic to organotypic hippocampal slices. Accordingly, 10 μM Cu(II) activated microglia in primary cell culture, which may also trigger neuronal damage.[63] Potential mechanisms for

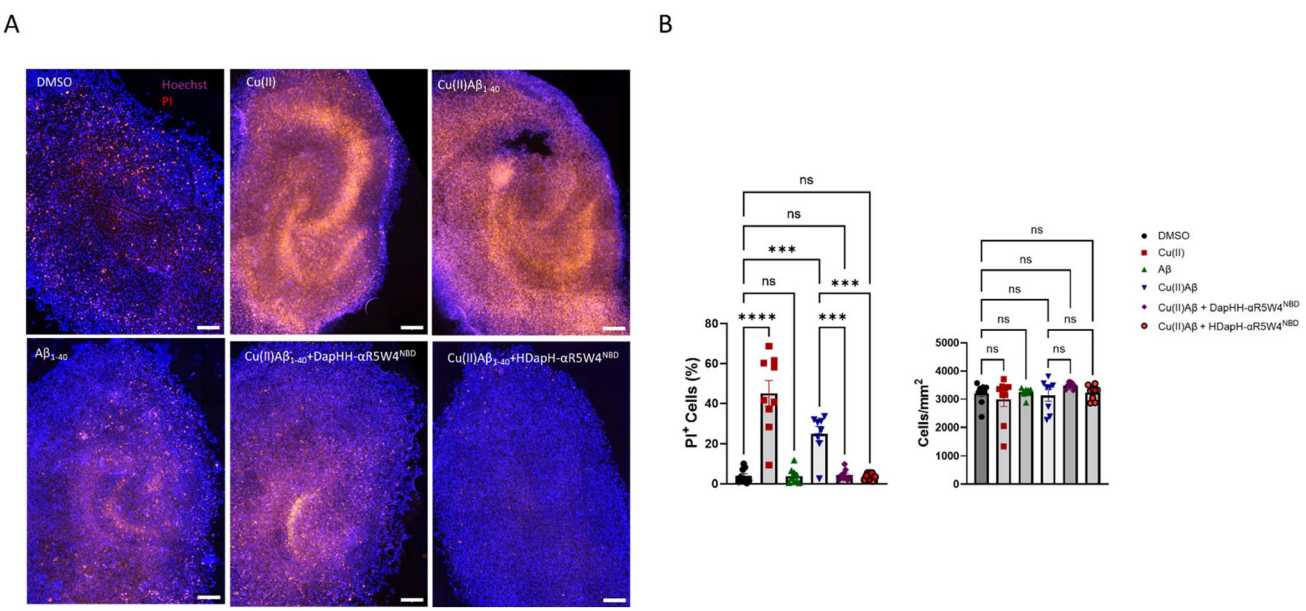

Fig. 4 DapHH-αR5W4^{NBD} or HDapH-αR5W4^{NBD} rescue Cu(II)-induced cell toxicity in OHSCs. (A) Representative images of the effect of Cu(II) peptide shuttles on Cu(II)(Aβ$_{1-40}$)-induced toxicity on OHSCs with (B) analysis of the preventive effect of DapHH-αR5W4^{NBD} or HDapH-αR5W4^{NBD} and analysis of the cell density in OHSC culture after 48 h treatment. Conditions: 10 μM Cu(II), DapHH-αR5W4^{NBD} or HDapH-αR5W4^{NBD}, 20 μM Aβ$_{40}$. Hoechst is blue and PI is red. Scale bar: 200 μm. A non-parametric test was carried out with a Kruskal–Wallis multiple comparison test for cells per mm^2. A parametric ordinary one-way ANOVA test was carried out with Tukey's multiple comparison test for PI$^+$ cells. ** $p < 0.01$, *** $p < 0.001$, **** $p < 0.0001$. $n = 3$ independent experiments with at least 3 slices per condition.

this Cu-induced toxicity include neuronal Cu overloading, Cu(Aβ)-induced ROS production in line with the endogenous presence of $AscH^-$ and microglial activation by "loosely"-bound extracellular Cu. Treatment with Cu(II)($A\beta_{1-40}$) or Cu(II)($A\beta_{1-42}$) also triggered an increase in slice toxicity, which could be attributed to similar mechanisms as those described for Cu(II) (Fig. 4, S11). Importantly, co-incubation with Cu(II)($A\beta_{1-40/42}$) and DapHH-αR5W4^{NBD} or HDapH-αR5W4^{NBD} completely rescued this toxicity. Together, these results are in line with our findings in PC12 cells and also reinforce the hypothesis that the Cu(II)($A\beta_{1-40/42}$)-induced toxicity arises from an extracellular effect. In other words, the toxicity observed in our assays is probably not the consequence of an increase in intracellular Cu levels, which is expected to be further increased by these Cu(II)-selective shuttles, but rather results from Cu(II)($A\beta_{1-40/42}$) ROS induction, which is rescued by the shuttles.

Proliferation and overactivation of microglia in the brain, concentrated around amyloid plaques, is a prominent feature of AD.[64] Given that Cu(II) could induce microglial activation both directly or through ROS production,[63,65,66] treated slices were stained with Iba1, a pan microglia marker,[67] and CD68, a marker of activated microglia.[68] Treatment of OHSC with Cu(II), Cu(II)$A\beta_{1-40}$ or Cu(II)$A\beta_{1-42}$ induced an increase in the percentage of microglial cells compared to DMSO-treated control slices (Fig. 5, S12). Since cell density remained unchanged after treatment with Cu(II)$A\beta_{1-40/42}$ (Fig. 5, S12), this could signify that the induced proliferation of microglial cells occurs concomitantly with the death of other cell types in Cu(II)-treated OHSC slices. Importantly, co-incubation with DapHH-αR5W4^{NBD} or HDapH-αR5W4^{NBD} reduced microglial cell proliferation induced by Cu(II)($A\beta_{1-40/42}$) (Fig. 5, S12). Equally, there was an increase in microglial activation in Cu(II), Cu(II)$A\beta_{1-40}$ or Cu(II)$A\beta_{1-42}$ treated slices, as seen by an increase in CD68 labelling in microglial cells (Iba1 and CD68 positive cells), which was efficiently prevented by co-incubating Cu(II)($A\beta_{1-40/42}$) treated slices with the Cu(II)-selective shuttles. In conclusion, DapHH-αR5W4^{NBD} and HDapH-αR5W4^{NBD} display protective activity towards brain tissue against Cu(II) and Cu(II)($A\beta_{1-40/42}$)-induced insult.

Discussion

Cu has been studied for its role in many pathologies such as Wilson's and Menkes diseases as well as several neurodegenerative disorders including AD.[69–80] Although the origins of Cu-related dysfunction have been elucidated in some cases (*e.g.* Wilson's disease and Menkes disease), many open questions remain, particularly concerning the mechanisms leading to Cu dyshomeostasis and how the loss of Cu homeostasis affects different organs, especially the brain.[81] In this context, tools to study Cu metabolism from cell culture to *in vivo* models are crucial to better delineate intrinsic mechanisms. To date, only a few studies have employed Cu(II)-selective fluo-

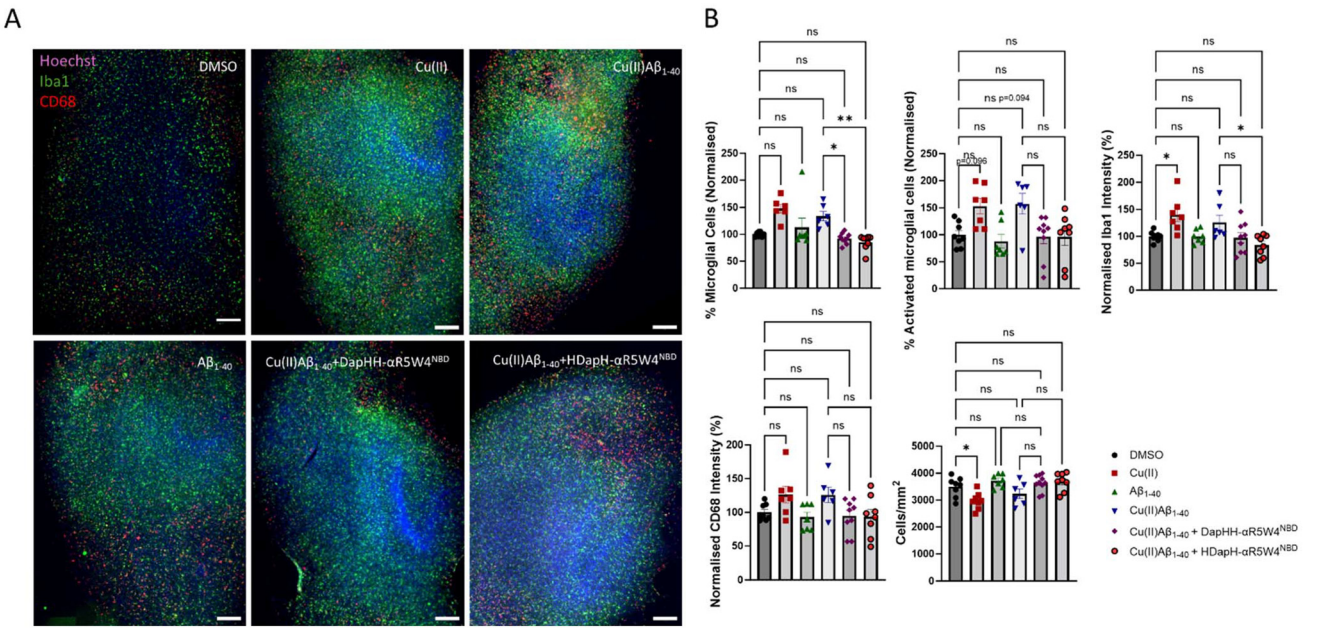

Fig. 5 Effect of DapHH-αR5W4^{NBD} or HDapH-αR5W4^{NBD} on Cu(II)-induced microglial proliferation and activation. (A) Representative images of the effect of Cu(II) peptide shuttles on Cu-induced Cu(II)$A\beta_{40}$ microglial activation on OHSCs with (B) analysis of the preventive effect of DapHH-αR5W4^{NBD} or HDapH-αR5W4^{NBD} on Cu(II)($A\beta_{1-40}$)-induced microglial proliferation and activation, and analysis of the cell density in OHSC culture after 48 h treatment. Hoechst is blue, Iba1 is green and CD68 is red. Scale bar: 200 μm. Conditions: 10 μM Cu(II) = DapHH-αR5W4^{NBD} or HDapH-αR5W4^{NBD}, 20 μM $A\beta_{1-40}$. A non-parametric test was carried out with a Kruskal–Wallis multiple comparison test for activated microglial cells and % microglial cells. A parametric ordinary one-way ANOVA test was carried out with Tukey's multiple comparison test for the rest, * $p < 0.05$, ** $p < 0.01$, *** $p < 0.001$, **** $p < 0.0001$. $n = 3$ independent experiments with at least 3 slices per condition.

rescence sensing probes capable of entering cells.[82,83] Although the molecules used in those studies cross cell membranes, they either display a very weak Cu(II) affinity or lack specificity, in contrast to the shuttles developed in the present work. A major advantage of the shuttles developed here is their ability to be tracked in real-time within cells. This is due to the positioning of a fluorophore close to the Cu(II) coordination sphere, which permits up to 98% fluorescence quenching upon Cu(II) binding (Fig. S2A). Hence, restoration of the shuttle fluorescence upon intracellular Cu release provides both temporal and subcellular resolutions of the Cu release process, making AKH-αR5W4^{NBD}, DapHH-αR5W4^{NBD} and HDapH-αR5W4^{NBD} particularly well-suited for mechanistic studies to follow Cu trafficking in cells.

Besides this first application, the shuttles described here were successfully designed to exhibit fast Cu(II)-binding kinetics, enabling efficient Cu(II) retrieval from Aβ (Fig. 1C and D). This property is essential because it permits the retrieval of extracellular Cu from Aβ before internalization into cells. The importance of this parameter is demonstrated in this study, as DapHH-αR5W4^{NBD} and HDapH-αR5W4^{NBD} immediately suppressed Cu(Aβ)-induced ROS production and protected both cells and tissue against Cu(II)–Aβ induced toxicity, in contrast to AKH-αR5W4^{NBD} (Fig. 3 and 4). Importantly, in our OHSC model, DapHH-αR5W4^{NBD} and HDapH-αR5W4^{NBD} were able to reverse the increased proliferation and activation of microglial cells after treatment with Cu(II) or Cu(II)(Aβ) (Fig. 5), both believed to be associated with brain toxicity provoked by Cu-induced ROS production.[68,84,85] Notwithstanding, our findings only demonstrate protection against Cu-induced injury and cannot be directly extrapolated to Aβ-driven neurodegeneration, as short time incubation with monomerized Aβ peptides alone did not induce toxicity in our OHSC model. Future studies in transgenic OHSC models that exhibit intrinsic Aβ toxicity will be essential.

Other important characteristics for good Cu shuttles are their intracellular kinetics, Cu release mechanism and intracellular location of Cu release. For instance, we showed here that nanomolar concentrations of Cu(II)GTSM (Fig. S6B) were toxic to PC12 cells, and the toxicity of Clioquinol has been previously reported.[86] It has equally been shown that Cu ionophores, such as Elesclomol, induced the so-called cuproptosis at low nanomolar concentrations, which was attributed to the Cu-induced aggregation of lipoylated mitochondrial proteins involved in the Krebs cycle.[87] These features may partially explain the failure of Cu ionophores, such as Clioquinol and PBT2 in clinical trials against AD, in addition to their lack of Cu(II) selectivity.[3,88] Another factor to be considered is the delivery site of these ionophores, which have tendencies to accumulate Cu in the mitochondria. The accumulation of Cu in the mitochondria might compete with other transition metal ions (mainly Fe) and provoke mitochondrial dysfunction as well as cuproptosis.[89] Hence, we expect that a slow and gradual release of Cu(II) from endolysosomal vesicles might be more beneficial and less toxic than fast cytosolic accumulation of Cu which might overwhelm the cellular metal ion buffering system.[90] Subsequently, the imported Cu can exit endosomes *via* CTR1/CTR2 or DMT1 transporters,[91,92] making Cu bioavailable as seen by ATP7A delocalization (Fig. 2B).

In line with this, we further hypothesized that the Cu release from the Cu shuttle described here occurs *via* thiol (ex: cystine or GSH) reduction in endosomes. In particular, *in cellulo* data indicated that HDapH-αR5W4^{NBD} releases Cu quicker into cells than DapHH-αR5W4^{NBD} (Fig. 2B, S9B). This correlates with the reduction kinetics of the Cu shuttles by GSH at acidic pH 5 (Fig. S8) but not at pH 7.4 (where DapHH-αR5W4^{NBD} is the fastest to be reduced). Hence, the progressive acidification along the endolysosomal pathway (the major cellular entry route used by αR5W4 CPP[39]) influences the kinetics of Cu release and reduction by GSH, in agreement with the pH-dependent speciation of the two shuttles.[44,93]

Conclusion

In conclusion, the Cu(II) peptide shuttles DapHH-αR5W4^{NBD} and HDapH-αR5W4^{NBD} bind Cu(II) with high affinity and selectivity and with sufficiently fast kinetics to suppress Cu(Aβ)-induced ROS production. These peptide shuttles efficiently retrieve extracellular Cu(II) from Aβ and import Cu into neuronal cells, displaying distinct kinetic profiles of Cu(II) extraction and release (AKH-αR5W4^{NBD}: slow binding and fast release; DapHH-αR5W4^{NBD}: intermittent binding and slow release; HDapH-αR5W4^{NBD}: fast binding and intermittent release). The Cu released within cells was further shown to be bioavailable and nontoxic. Importantly, these Cu(II) peptide shuttles also prevented Cu- and Cu(Aβ)-induced neurotoxicity, microglial proliferation and activation in OHSCs. Therefore, they pose as promising drug candidates for future *in vivo* studies in AD animal models and could lead to therapeutic strategies aimed at correcting Cu-dyshomeostasis in patients with deregulated Cu levels.

Conflicts of interest

The authors declare that they have no conflicts of interest with the contents of this article.

Data availability

All data will be made available upon request to the corresponding authors.

Supplementary information (SI) is available. See DOI: https://doi.org/10.1039/d6qi00862c.

Acknowledgements

This work was supported by a grant to N.V. from ITI Neurostra as part of the IdEx Unistra (ANR-10-IDEX-0002) under the framework of the French Program Investments for the Future.

The IdEx PhD program, University of Strasbourg and the ITI Neurostra program (ANR-10-IDEX-0002) provided salary to MO, and INSERM is providing salary to NV and SG. We acknowledge the Plateforme Imagerie In Vitro of ITI Neurostra at CNRS UAR-3256. Special thanks to Fréderic Doussau for his help with OHSCs.

References

1 E. Falcone, M. Okafor, N. Vitale, L. Raibaut, A. Sour and P. Faller, Extracellular Cu2+ Pools and Their Detection: From Current Knowledge to next-Generation Probes, *Coord. Chem. Rev.*, 2021, **433**, 213727, DOI: **10.1016/j.ccr.2020.213727**.

2 N. J. Robinson and D. R. Winge, Copper Metallochaperones, *Annu. Rev. Biochem.*, 2010, **79**(1), 537–562, DOI: **10.1146/annurev-biochem-030409-143539**.

3 J. F. Quinn, S. Crane, C. Harris and T. L. Wadsworth, Copper in Alzheimer's Disease: Too Much or Too Little?, *Expert Rev. Neurother.*, 2009, **9**(5), 631–637, DOI: **10.1586/ern.09.27**.

4 L. Wang, Y.-L. Yin, X.-Z. Liu, P. Shen, Y.-G. Zheng, X.-R. Lan, C.-B. Lu and J.-Z. Wang, Current Understanding of Metal Ions in the Pathogenesis of Alzheimer's Disease, *Transl. Neurodegener.*, 2020, **9**(1), 10, DOI: **10.1186/s40035-020-00189-z**.

5 K. Voss, C. Harris, M. Ralle, M. Duffy, C. Murchison and J. F. Quinn, Modulation of Tau Phosphorylation by Environmental Copper, *Transl. Neurodegener.*, 2014, **3**(1), 24, DOI: **10.1186/2047-9158-3-24**.

6 M. Scholefield, S. J. Church, J. Xu, S. Kassab, N. J. Gardiner, F. Roncaroli, N. M. Hooper, R. D. Unwin and G. J. S. Cooper, Evidence That Levels of Nine Essential Metals in Post-Mortem Human-Alzheimer's-Brain and Ex Vivo Rat-Brain Tissues Are Unaffected by Differences in Post-Mortem Delay, Age, Disease Staging, and Brain Bank Location†, *Metallomics*, 2020, **12**(6), 952–962, DOI: **10.1039/d0mt00048e**.

7 M. Schrag, C. Mueller, U. Oyoyo, M. A. Smith and W. M. Kirsch, Iron, Zinc and Copper in the Alzheimer's Disease Brain: A Quantitative Meta-Analysis. Some Insight on the Influence of Citation Bias on Scientific Opinion, *Prog. Neurobiol.*, 2011, **94**(3), 296–306, DOI: **10.1016/j.pneurobio.2011.05.001**.

8 D.-D. Li, W. Zhang, Z.-Y. Wang and P. Zhao, Serum Copper, Zinc, and Iron Levels in Patients with Alzheimer's Disease: A Meta-Analysis of Case-Control Studies, *Front. Aging Neurosci.*, 2017, **9**, 300, DOI: **10.3389/fnagi.2017.00300**.

9 R. Squitti, C. Cataldi, L. Gigante, M. Marianetti, M. Rosari, S. Mariani, S. Bucossi, G. Mastromoro, M. Ventriglia, I. Simonelli, V. Tondolo, P. Singh, A. Kumar, A. Pal and M. Rongioletti, Non-Ceruloplasmin Copper Identifies a Subtype of Alzheimer's Disease (CuAD): Characterization of the Cognitive Profile and Case of a CuAD Patient Carrying an RGS7 Stop-Loss Variant, *Int. J. Mol. Sci.*, 2023, **24**(7), 6377, DOI: **10.3390/ijms24076377**.

10 R. Squitti, M. Ventriglia, I. Simonelli, C. Bonvicini, A. Costa, G. Perini, G. Binetti, L. Benussi, R. Ghidoni, G. Koch, B. Borroni, A. Albanese, S. L. Sensi and M. Rongioletti, Copper Imbalance in Alzheimer's Disease: Meta-Analysis of Serum, Plasma, and Brain Specimens, and Replication Study Evaluating ATP7B Gene Variants, *Biomolecules*, 2021, **11**(7), 960, DOI: **10.3390/biom11070960**.

11 S. A. James, I. Volitakis, P. A. Adlard, J. A. Duce, C. L. Masters, R. A. Cherny and A. I. Bush, Elevated Labile Cu Is Associated with Oxidative Pathology in Alzheimer Disease, *Free Radicals Biol. Med.*, 2012, **52**(2), 298–302, DOI: **10.1016/j.freeradbiomed.2011.10.446**.

12 A. Rembach, D. J. Hare, M. Lind, C. J. Fowler, R. A. Cherny, C. McLean, A. I. Bush, C. L. Masters and B. R. Roberts, Decreased Copper in Alzheimer's Disease Brain Is Predominantly in the Soluble Extractable Fraction, *Int. J. Alzheimer's Dis.*, 2013, **2013**, e623241, DOI: **10.1155/2013/623241**.

13 L. M. Miller, Q. Wang, T. P. Telivala, R. J. Smith, A. Lanzirotti and J. Miklossy, Synchrotron-Based Infrared and X-Ray Imaging Shows Focalized Accumulation of Cu and Zn Co-Localized with Beta-Amyloid Deposits in Alzheimer's Disease, *J. Struct. Biol.*, 2006, **155**(1), 30–37, DOI: **10.1016/j.jsb.2005.09.004**.

14 M. Schrag, C. Mueller, U. Oyoyo and W. M. Kirsch, Iron, Zinc and Copper in the Alzheimer's Disease Brain: A Quantitative Meta-Analysis. Some Insight on the Influence of Citation Bias on Scientific Opinion, *Prog. Neurobiol.*, 2011, **94**(3), 296–306, DOI: **10.1016/j.pneurobio.2011.05.001**.

15 Y. Tian, Q. Shang, R. Liang and J. H. Viles, Copper(II) Can Kinetically Trap Arctic and Italian Amyloid-B40 as Toxic Oligomers, Mimicking Cu(II) Binding to Wild-Type Amyloid-B42: Implications for Familial Alzheimer's Disease, *JACS Au*, 2024, **4**(2), 578–591, DOI: **10.1021/jacsau.3c00687**.

16 A. Abelein, S. Ciofi-Baffoni, C. Mörman, R. Kumar, A. Giachetti, M. Piccioli and H. Biverstål, Molecular Structure of Cu(II)-Bound Amyloid-β Monomer Implicated in Inhibition of Peptide Self-Assembly in Alzheimer's Disease, *JACS Au*, 2022, **2**(11), 2571–2584, DOI: **10.1021/jacsau.2c00438**.

17 C. Cheignon, M. Tomas, D. Bonnefont-Rousselot, P. Faller, C. Hureau and F. Collin, Oxidative Stress and the Amyloid Beta Peptide in Alzheimer's Disease, *Redox Biol.*, 2018, **14**, 450–464, DOI: **10.1016/j.redox.2017.10.014**.

18 E. Atrián-Blasco, P. Gonzalez, A. Santoro, B. Alies, P. Faller and C. Hureau, Cu and Zn Coordination to Amyloid Peptides: From Fascinating Chemistry to Debated Pathological Relevance, *Coord. Chem. Rev.*, 2018, **375**, 38–55, DOI: **10.1016/j.ccr.2018.04.007**.

19 E. Falcone and C. Hureau, Redox Processes in Cu-Binding Proteins: The "in-between" States in Intrinsically Disordered Peptides, *Chem. Soc. Rev.*, 2023, **52**(19), 6595–6600, DOI: **10.1039/D3CS00443K**.

20 A. R. White, K. J. Barnham and A. I. Bush, Metal Homeostasis in Alzheimer's Disease, *Expert Rev. Neurother.*, 2006, **6**(5), 711–722, DOI: 10.1586/14737175.6.5.711.

21 S. Bagheri, R. Squitti, T. Haertlé, M. Siotto and A. A. Saboury, Role of Copper in the Onset of Alzheimer's Disease Compared to Other Metals, *Front. Aging Neurosci.*, 2018, **9**, 446, DOI: 10.3389/fnagi.2017.00446.

22 C. S. Atwood, G. Perry, H. Zeng, Y. Kato, W. D. Jones, K.-Q. Ling, X. Huang, R. D. Moir, D. Wang, L. M. Sayre, M. A. Smith, S. G. Chen and A. I. Bush, Copper Mediates Dityrosine Cross-Linking of Alzheimer's Amyloid-β, *Biochemistry*, 2004, **43**(2), 560–568, DOI: 10.1021/bi0358824.

23 C. Cheignon, F. Collin, L. Sabater and C. Hureau, Oxidative Damages on the Alzheimer's Related-Aβ Peptide Alters Its Ability to Assemble, *Antioxidants*, 2023, **12**(2), 472, DOI: 10.3390/antiox12020472.

24 L. Jenagaratnam and R. McShane, Clioquinol for the Treatment of Alzheimer's Disease, *Cochrane Database Syst. Rev.*, 2006, **1**, CD005380, DOI: 10.1002/14651858.CD005380.pub2.

25 E. L. Sampson, L. Jenagaratnam and R. McShane, Metal Protein Attenuating Compounds for the Treatment of Alzheimer's Dementia, *Cochrane Database Syst. Rev.*, 2014, **2**, CD005380, DOI: 10.1002/14651858.CD005380.pub5.

26 A. R. White, T. Du, K. M. Laughton, I. Volitakis, R. A. Sharples, M. E. Xilinas, D. E. Hoke, R. M. D. Holsinger, G. Evin, R. A. Cherny, A. F. Hill, K. J. Barnham, Q.-X. Li, A. I. Bush and C. L. Masters, Degradation of the Alzheimer Disease Amyloid β-Peptide by Metal-Dependent Up-Regulation of Metalloprotease Activity*, *J. Biol. Chem.*, 2006, **281**(26), 17670–17680, DOI: 10.1074/jbc.M602487200.

27 P. J. Crouch, L. W. Hung, P. A. Adlard, M. Cortes, V. Lal, G. Filiz, K. A. Perez, M. Nurjono, A. Caragounis, T. Du, K. Laughton, I. Volitakis, A. I. Bush, Q.-X. Li, C. L. Masters, R. Cappai, R. A. Cherny, P. S. Donnelly, A. R. White and K. J. Barnham, Increasing Cu Bioavailability Inhibits Abeta Oligomers and Tau Phosphorylation, *Proc. Natl. Acad. Sci. U. S. A.*, 2009, **106**(2), 381–386, DOI: 10.1073/pnas.0809057106.

28 R. A. Cherny, C. S. Atwood, M. E. Xilinas, D. N. Gray, W. D. Jones, C. A. McLean, K. J. Barnham, I. Volitakis, F. W. Fraser, Y.-S. Kim, X. Huang, L. E. Goldstein, R. D. Moir, J. T. Lim, K. Beyreuther, H. Zheng, R. E. Tanzi, C. L. Masters and A. I. Bush, Treatment with a Copper-Zinc Chelator Markedly and Rapidly Inhibits β-Amyloid Accumulation in Alzheimer's Disease Transgenic Mice, *Neuron*, 2001, **30**(3), 665–676, DOI: 10.1016/S0896-6273(01)00317-8.

29 C. W. Ritchie, A. I. Bush, A. Mackinnon, S. Macfarlane, M. Mastwyk, L. MacGregor, L. Kiers, R. Cherny, Q.-X. Li, A. Tammer, D. Carrington, C. Mavros, I. Volitakis, M. Xilinas, D. Ames, S. Davis, K. Beyreuther, R. E. Tanzi and C. L. Masters, Metal-Protein Attenuation with Iodochlorhydroxyquin (Clioquinol) Targeting Abeta Amyloid Deposition and Toxicity in Alzheimer Disease: A Pilot Phase 2 Clinical Trial, *Arch. Neurol.*, 2003, **60**(12), 1685–1691, DOI: 10.1001/archneur.60.12.1685.

30 M. L. Hegde, P. Bharathi, A. Suram, C. Venugopal, R. Jagannathan, P. Poddar, P. Srinivas, K. Sambamurti, K. J. Rao, J. Scancar, L. Messori, L. Zecca and P. Zatta, Challenges Associated with Metal Chelation Therapy in Alzheimer's Disease, *J. Alzheimer's Dis.*, 2009, **17**(3), 457–468, DOI: 10.3233/JAD-2009-1068.

31 M. S. Yassin, J. Ekblom, M. Xilinas, C. G. Gottfries and L. Oreland, Changes in Uptake of Vitamin B(12) and Trace Metals in Brains of Mice Treated with Clioquinol, *J. Neurol. Sci.*, 2000, **173**(1), 40–44, DOI: 10.1016/s0022-510x(99)00297-x.

32 N. G. Faux, C. W. Ritchie, A. Gunn, A. Rembach, A. Tsatsanis, J. Bedo, J. Harrison, L. Lannfelt, K. Blennow, H. Zetterberg, M. Ingelsson, C. L. Masters, R. E. Tanzi, J. L. Cummings, C. M. Herd and A. I. Bush, PBT2 Rapidly Improves Cognition in Alzheimer's Disease: Additional Phase II Analyses, *J. Alzheimer's Dis.*, 2010, **20**(2), 509–516, DOI: 10.3233/JAD-2010-1390.

33 L. M. Guthrie, S. Soma, S. Yuan, A. Silva, M. Zulkifli, T. C. Snavely, H. F. Greene, E. Nunez, B. Lynch, C. De Ville, V. Shanbhag, F. R. Lopez, A. Acharya, M. J. Petris, B.-E. Kim, V. M. Gohil and J. C. Sacchettini, Elesclomol Alleviates Menkes Pathology and Mortality by Escorting Cu to Cuproenzymes in Mice, *Science*, 2020, **368**(6491), 620–625, DOI: 10.1126/science.aaz8899.

34 P. S. Donnelly, A. Caragounis, T. Du, K. M. Laughton, I. Volitakis, R. A. Cherny, R. A. Sharples, A. F. Hill, Q.-X. Li, C. L. Masters, K. J. Barnham and A. R. White, Selective Intracellular Release of Copper and Zinc Ions from Bis(Thiosemicarbazonato) Complexes Reduces Levels of Alzheimer Disease Amyloid-β Peptide*, *J. Biol. Chem.*, 2008, **283**(8), 4568–4577, DOI: 10.1074/jbc.M705957200.

35 M. Okafor, P. Gonzalez, P. Ronot, I. E. Masoudi, A. Boos, S. Ory, S. Chasserot-Golaz, S. Gasman, L. Raibaut, C. Hureau, N. Vitale and P. Faller, Development of Cu(II)-Specific Peptide Shuttles Capable of Preventing Cu–Amyloid Beta Toxicity and Importing Bioavailable Cu into Cells, *Chem. Sci.*, 2022, **13**(40), 11829–11840, DOI: 10.1039/D2SC02593K.

36 J. Smeyers-Verbeke, E. Defrise-Gussenhoven, G. Ebinger, A. Löwenthal and D. L. Massart, Distribution of Cu and Zn in Human Brain Tissue, *Clin. Chim. Acta*, 1974, **51**(3), 309–314, DOI: 10.1016/0009-8981(74)90317-9.

37 R. Sankararamakrishnan, S. Verma and S. Kumar, ATCUN-like Metal-Binding Motifs in Proteins: Identification and Characterization by Crystal Structure and Sequence Analysis, *Proteins*, 2005, **58**(1), 211–221, DOI: 10.1002/prot.20265.

38 A. Walrant, A. Bauzá, C. Girardet, I. D. Alves, S. Lecomte, F. Illien, S. Cardon, N. Chaianantakul, M. Pallerla, F. Burlina, A. Frontera and S. Sagan, Ionpair-π Interactions Favor Cell Penetration of Arginine/Tryptophan-Rich Cell-Penetrating Peptides, *Biochim. Biophys. Acta, Biomembr.*, 2020, **1862**(2), 183098, DOI: 10.1016/j.bbamem.2019.183098.

39 M. Okafor, O. Champomier, L. Raibaut, S. Ozkan, N. E. Kholti, S. Ory, S. Chasserot-Golaz, S. Gasman, C. Hureau, P. Faller and N. Vitale, Restoring Cellular Copper Homeostasis in Alzheimer Disease: A Novel Peptide Shuttle Is Internalized by an ATP-Dependent Endocytosis Pathway Involving Rab5-and Rab14endosomes, *Front. Mol. Biosci.*, 2024, **11**, 1355963, DOI: 10.3389/fmolb.2024.1355963.

40 N. Thieriet, J. Alsina, E. Giralt, F. Guibé and F. Albericio, Use of Alloc-Amino Acids in Solid-Phase Peptide Synthesis. Tandem Deprotection-Coupling Reactions Using Neutral Conditions, *Tetrahedron Lett.*, 1997, **38**(41), 7275–7278, DOI: 10.1016/S0040-4039(97)01690-0.

41 B. Zhang-Haagen, R. Biehl, L. Nagel-Steger, A. Radulescu, D. Richter and D. Willbold, Monomeric Amyloid Beta Peptide in Hexafluoroisopropanol Detected by Small Angle Neutron Scattering, *PLoS One*, 2016, **11**(2), e0150267, DOI: 10.1371/journal.pone.0150267.

42 E. Tanguy, P. Costé de Bagneaux, N. Kassas, M.-R. Ammar, Q. Wang, A.-M. Haeberlé, J. Raherindratsara, L. Fouillen, P.-Y. Renard, M. Montero-Hadjadje, S. Chasserot-Golaz, S. Ory, S. Gasman, M.-F. Bader and N. Vitale, Mono- and Poly-Unsaturated Phosphatidic Acid Regulate Distinct Steps of Regulated Exocytosis in Neuroendocrine Cells, *Cell Rep.*, 2020, **32**(7), 108026, DOI: 10.1016/j.celrep.2020.108026.

43 L. Stoppini, P.-A. Buchs and D. Muller, A Simple Method for Organotypic Cultures of Nervous Tissue, *J. Neurosci. Methods*, 1991, **37**(2), 173–182, DOI: 10.1016/0165-0270(91)90128-M.

44 M. Lefèvre, K. P. Malikidogo, C. Esmieu and C. Hureau, Sequence–Activity Relationship of ATCUN Peptides in the Context of Alzheimer's Disease, *Molecules*, 2022, **27**(22), 7903, DOI: 10.3390/molecules27227903.

45 P. Gonzalez, B. Vileno, K. Bossak, Y. El Khoury, P. Hellwig, W. Bal, C. Hureau and P. Faller, Cu(II) Binding to the Peptide Ala-His-His, a Chimera of the Canonical Cu(II)-Binding Motifs Xxx-His and Xxx-Zzz-His, *Inorg. Chem.*, 2017, **56**(24), 14870–14879, DOI: 10.1021/acs.inorgchem.7b01996.

46 A. Conte-Daban, V. Borghesani, S. Sayen, E. Guillon, Y. Journaux, G. Gontard, L. Lisnard and C. Hureau, Link between Affinity and Cu(II) Binding Sites to Amyloid-β Peptides Evaluated by a New Water-Soluble UV–Visible Ratiometric Dye with a Moderate Cu(II) Affinity, *Anal. Chem.*, 2017, **89**(3), 2155–2162, DOI: 10.1021/acs.analchem.6b04979.

47 M. Mital, N. E. Wezynfeld, T. Frączyk, M. Z. Wiloch, U. E. Wawrzyniak, A. Bonna, C. Tumpach, K. J. Barnham, C. L. Haigh, W. Bal and S. C. Drew, A Functional Role for Aβ in Metal Homeostasis? N-Truncation and High-Affinity Copper Binding, *Angew. Chem., Int. Ed.*, 2015, **54**(36), 10460–10464, DOI: 10.1002/anie.201502644.

48 C. Grundschober, M. L. Malosio, L. Astolfi, T. Giordano, P. Nef and J. Meldolesi, Neurosecretion Competence., A Comprehensive Gene Expression Program Identified in PC12 Cells, *J. Biol. Chem.*, 2002, **277**(39), 36715–36724, DOI: 10.1074/jbc.M203777200.

49 S. G. Kaler, ATP7A-Related Copper Transport Diseases—Emerging Concepts and Future Trends, *Nat. Rev. Neurol.*, 2011, **7**(1), 15–29, DOI: 10.1038/nrneurol.2010.180.

50 M. E. Rice, M. E. Rice and M. E. Rice, Ascorbate Regulation and Its Neuroprotective Role in the Brain, *Trends Neurosci.*, 2000, **23**(5), 209–216, DOI: 10.1016/S0166-2236(99)01543-X.

51 L. Guilloreau, S. Combalbert, A. Sournia-Saquet, H. Mazarguil and P. Faller, Redox Chemistry of Copper-Amyloid-Beta: The Generation of Hydroxyl Radical in the Presence of Ascorbate Is Linked to Redox-Potentials and Aggregation State, *ChemBioChem*, 2007, **8**(11), 1317–1325, DOI: 10.1002/cbic.200700111.

52 F. E. Harrison and J. M. May, Vitamin C Function in the Brain: Vital Role of the Ascorbate Transporter SVCT2, *Free Radicals Biol. Med.*, 2009, **46**(6), 719–730, DOI: 10.1016/j.freeradbiomed.2008.12.018.

53 P. Faller and C. Hureau, Reproducibility Problems of Amyloid-β Self-Assembly and How to Deal With Them, *Front. Chem.*, 2021, **8**, 611227, DOI: 10.3389/fchem.2020.611227.

54 A. E. Feller, Technic and Application of Roller Tube Cultures, in *Handbuch der Virusforschung: II. Ergänzungsband*, ed. R. Doerr, C. Hallauer, F. M. Burnet, M. D. Eaton, A. E. Feller, E. W. Flosdorf, Th. Francis, M. Kaiser, H. Ruska and P. Vonwiller, Springer, Vienna, 1950, pp. 1–10. DOI: 10.1007/978-3-7091-5688-9_1.

55 S. Wray, Organotypic Slice Explant Roller-Tube Cultures, in *Practical Cell Culture Techniques*, ed. A. A. Boulton, G. B. Baker and W. Walz, Neuromethods, Humana Press, Totowa, NJ, 1992, pp. 201–239. DOI: 10.1385/0-89603-214-0:201.

56 E. C. Suh, Y. J. Jung, Y. A. Kim, E. M. Park and K. E. Lee, Aβ25–35 Induces Presynaptic Changes in Organotypic Hippocampal Slice Cultures, *NeuroToxicology*, 2008, **29**(4), 691–699, DOI: 10.1016/j.neuro.2008.04.001.

57 R. L. Frozza, A. P. Horn, J. B. Hoppe, F. Simão, D. Gerhardt, R. A. Comiran and C. G. Salbego, A Comparative Study of β-Amyloid Peptides Aβ1–42 and Aβ25–35 Toxicity in Organotypic Hippocampal Slice Cultures, *Neurochem. Res.*, 2009, **34**(2), 295–303, DOI: 10.1007/s11064-008-9776-8.

58 A. J. Bruce, B. Malfroy and M. Baudry, Beta-Amyloid Toxicity in Organotypic Hippocampal Cultures: Protection by EUK-8, a Synthetic Catalytic Free Radical Scavenger, *Proc. Natl. Acad. Sci. U. S. A.*, 1996, **93**(6), 2312–2316, DOI: 10.1073/pnas.93.6.2312.

59 K. L. Clapp-Lilly, M. A. Smith, G. Perry, P. L. Harris, X. Zhu and L. K. Duffy, Melatonin Acts as Antioxidant and Pro-Oxidant in an Organotypic Slice Culture Model of Alzheimer's Disease, *NeuroReport*, 2001, **12**(6), 1277.

60 M. Richter, N. Vidovic, K. Biber, A. Dolga, C. Culmsee and R. Dodel, The Neuroprotective Role of Microglial Cells against Amyloid Beta-Mediated Toxicity in Organotypic Hippocampal Slice Cultures, *Brain Pathol.*, 2020, **30**(3), 589–602, DOI: 10.1111/bpa.12807.

61 R. Novotny, F. Langer, J. Mahler, A. Skodras, A. Vlachos, B. M. Wegenast-Braun, S. A. Kaeser, J. J. Neher, Y. S. Eisele,

M. J. Pietrowski, K. P. R. Nilsson, T. Deller, M. Staufenbiel, B. Heimrich and M. Jucker, Conversion of Synthetic Aβ to In Vivo Active Seeds and Amyloid Plaque Formation in a Hippocampal Slice Culture Model, *J. Neurosci.*, 2016, **36**(18), 5084–5093, DOI: 10.1523/JNEUROSCI.0258-16.2016.

62 T. Chepda, M. Cadau, P. Girin, J. Frey and A. Chamson, Monitoring of Ascorbate at a Constant Rate in Cell Culture: Effect on Cell Growth, *In Vitro Cell. Dev. Biol.: Anim.*, 2001, **37**(1), 26–30, DOI: 10.1290/1071-2690(2001)037%3C0026:MOAAAC%3E2.0.CO;2.

63 Z. Hu, F. Yu, P. Gong, Y. Qiu, W. Zhou, Y. Cui, J. Li and H. Chen, Subneurotoxic Copper(II)-Induced NF-κB-Dependent Microglial Activation Is Associated with Mitochondrial ROS, *Toxicol. Appl. Pharmacol.*, 2014, **276**(2), 95–103, DOI: 10.1016/j.taap.2014.01.020.

64 D. V. Hansen, J. E. Hanson and M. Sheng, Microglia in Alzheimer's Disease, *J. Cell Biol.*, 2018, **217**(2), 459–472, DOI: 10.1083/jcb.201709069.

65 L. Yan, S. Liu, C. Wang, F. Wang, Y. Song, N. Yan, S. Xi, Z. Liu and G. Sun, JNK and NADPH Oxidase Involved in Fluoride-Induced Oxidative Stress in BV-2 Microglia Cells, *Mediators Inflammation*, 2013, **2013**, e895975, DOI: 10.1155/2013/895975.

66 D. S. A. Simpson and P. L. Oliver, ROS Generation in Microglia: Understanding Oxidative Stress and Inflammation in Neurodegenerative Disease, *Antioxidants*, 2020, **9**(8), 743, DOI: 10.3390/antiox9080743.

67 D. Ito, Y. Imai, K. Ohsawa, K. Nakajima, Y. Fukuuchi and S. Kohsaka, Microglia-Specific Localisation of a Novel Calcium Binding Protein, Iba1, *Mol. Brain Res.*, 1998, **57**(1), 1–9, DOI: 10.1016/S0169-328X(98)00040-0.

68 K. E. Hopperton, D. Mohammad, M. O. Trépanier, V. Giuliano and R. P. Bazinet, Markers of Microglia in Post-Mortem Brain Samples from Patients with Alzheimer's Disease: A Systematic Review, *Mol. Psychiatry*, 2018, **23**(2), 177–198, DOI: 10.1038/mp.2017.246.

69 I. Sirangelo and C. Iannuzzi, The Role of Metal Binding in the Amyotrophic Lateral Sclerosis-Related Aggregation of Copper-Zinc Superoxide Dismutase, *Molecules*, 2017, **22**(9), 1429, DOI: 10.3390/molecules22091429.

70 L. J. Hayward, J. A. Rodriguez, J. W. Kim, A. Tiwari, J. J. Goto, D. E. Cabelli, J. S. Valentine and R. H. Brown, Decreased Metallation and Activity in Subsets of Mutant Superoxide Dismutases Associated with Familial Amyotrophic Lateral Sclerosis, *J. Biol. Chem.*, 2002, **277**(18), 15923–15931, DOI: 10.1074/jbc.M112087200.

71 K. M. Davies, D. J. Hare, V. Cottam, N. Chen, L. Hilgers, G. Halliday, J. F. B. Mercer and K. L. Double, Localization of Copper and Copper Transporters in the Human Brain†, *Metallomics*, 2013, **5**(1), 43–51, DOI: 10.1039/c2mt20151h.

72 S. Genoud, B. R. Roberts, A. P. Gunn, G. M. Halliday, S. J. G. Lewis, H. J. Ball, D. J. Hare and K. L. Double, Subcellular Compartmentalisation of Copper, Iron, Manganese, and Zinc in the Parkinson's Disease Brain, *Metallomics*, 2017, **9**(10), 1447–1455, DOI: 10.1039/c7mt00244k.

73 D. T. Dexter, A. Carayon, F. Javoy-Agid, Y. Agid, F. R. Wells, S. E. Daniel, A. J. Lees, P. Jenner and C. D. Marsden, Alterations in the Levels of Iron, Ferritin and Other Trace Metals in Parkinson's Disease and Other Neurodegenerative Diseases Affecting the Basal Ganglia, *Brain*, 1991, **114**(4), 1953–1975, DOI: 10.1093/brain/114.4.1953.

74 B. F. G. Popescu, M. J. George, U. Bergmann, A. V. Garachtchenko, M. E. Kelly, R. P. E. McCrea, K. Lüning, R. M. Devon, G. N. George, A. D. Hanson, S. M. Harder, L. D. Chapman, I. J. Pickering and H. Nichol, Mapping Metals in Parkinson's and Normal Brain Using Rapid-Scanning x-Ray Fluorescence, *Phys. Med. Biol.*, 2009, **54**(3), 651, DOI: 10.1088/0031-9155/54/3/012.

75 S. Ayton, P. Lei, J. A. Duce, B. X. W. Wong, A. Sedjahtera, P. A. Adlard, A. I. Bush and D. I. Finkelstein, Ceruloplasmin Dysfunction and Therapeutic Potential for Parkinson Disease, *Ann. Neurol.*, 2013, **73**(4), 554–559, DOI: 10.1002/ana.23817.

76 P. Hedera, Wilson's Disease: A Master of Disguise, *Parkinsonism Relat. Disord.*, 2019, **59**, 140–145, DOI: 10.1016/j.parkreldis.2019.02.016.

77 A. Nagral, M. S. Sarma, J. Matthai, P. L. Kukkle, H. Devarbhavi, S. Sinha, S. Alam, A. Bavdekar, R. K. Dhiman, C. E. Eapen, V. Goyal, N. Mohan, R. M. Kandadai, M. Sathiyasekaran, U. Poddar, A. Sibal, S. Sankaranarayanan, A. Srivastava, B. R. Thapa, P. M. Wadia, S. K. Yachha and A. Dhawan, Wilson's Disease: Clinical Practice Guidelines of the Indian National Association for Study of the Liver, the Indian Society of Pediatric Gastroenterology, Hepatology and Nutrition, and the Movement Disorders Society of India, *J. Clin. Exp. Hepatol.*, 2019, **9**(1), 74–98, DOI: 10.1016/j.jceh.2018.08.009.

78 J. Pfeiffenberger, C. M. Lohse, D. Gotthardt, C. Rupp, M. Weiler, U. Teufel, K. H. Weiss and A. Gauss, Long-Term Evaluation of Urinary Copper Excretion and Non-Caeruloplasmin Associated Copper in Wilson Disease Patients under Medical Treatment, *J. Inherited Metab. Dis.*, 2019, **42**(2), 371–380, DOI: 10.1002/jimd.12046.

79 P. R. Kollros, R. D. Dick and G. J. Brewer, Correction of Cerebrospinal Fluid Copper in Menkes Kinky Hair Disease, *Pediatr. Neurol.*, 1991, **7**(4), 305–307, DOI: 10.1016/0887-8994(91)90052-m.

80 Z. Tümer and L. B. Møller, Menkes Disease, *Eur. J. Hum. Genet.*, 2010, **18**(5), 511–518, DOI: 10.1038/ejhg.2009.187.

81 M. Okafor, P. Faller and N. Vitale, Cell-Specific Copper Dyshomeostasis Mechanism in Alzheimer's Disease, *Transl. Neurodegener.*, 2025, **14**(1), 42, DOI: 10.1186/s40035-025-00504-6.

82 G. Donadio, R. Di Martino, R. Oliva, L. Petraccone, P. Del Vecchio, B. Di Luccia, E. Ricca, R. Isticato, A. Di Donato and E. Notomista, A New Peptide-Based Fluorescent Probe Selective for Zinc(II) and Copper(II), *J. Mater. Chem. B*, 2016, **4**(43), 6979–6988, DOI: 10.1039/c6tb00671j.

83 Y. Hu, A. Chen, Z. Kong and D. Sun, A Reversible Colorimetric and Fluorescence "Turn-Off" Chemosensor for Detection of Cu2+ and Its Application in Living Cell

Imaging, *Molecules*, 2019, **24**(23), 4283, DOI: **10.3390/molecules24234283**.

84 C. Cheignon, M. Tomas, D. Bonnefont-Rousselot, P. Faller, C. Hureau and F. Collin, Oxidative Stress and the Amyloid Beta Peptide in Alzheimer's Disease, *Redox Biol.*, 2017, **14**, 450–464, DOI: **10.1016/j.redox.2017.10.014**.

85 R. Patel and M. Aschner, Commonalities between Copper Neurotoxicity and Alzheimer's Disease, *Toxics*, 2021, **9**(1), 4, DOI: **10.3390/toxics9010004**.

86 L. Benvenisti-Zarom, J. Chen and R. F. Regan, The Oxidative Neurotoxicity of Clioquinol, *Neuropharmacology*, 2005, **49**(5), 687–694, DOI: **10.1016/j.neuropharm.2005.04.023**.

87 P. Tsvetkov, S. Coy, B. Petrova, M. Dreishpoon, A. Verma, M. Abdusamad, J. Rossen, L. Joesch-Cohen, R. Humeidi, R. D. Spangler, J. K. Eaton, E. Frenkel, M. Kocak, S. M. Corsello, S. Lutsenko, N. Kanarek, S. Santagata and T. R. Golub, Copper Induces Cell Death by Targeting Lipoylated TCA Cycle Proteins, *Science*, 2022, **375**(6586), 1254–1261, DOI: **10.1126/science.abf0529**.

88 J. L. Arbiser, S.-K. Kraeft, R. van Leeuwen, S. J. Hurwitz, M. Selig, G. R. Dickersin, A. Flint, H. R. Byers and L. B. Chen, Clioquinol-Zinc Chelate: A Candidate Causative Agent of Subacute Myelo-Optic Neuropathy, *Mol. Med.*, 1998, **4**(10), 665–670, DOI: **10.1007/BF03401927**.

89 C. Vallières, S. L. Holland and S. V. Avery, Mitochondrial Ferredoxin Determines Vulnerability of Cells to Copper Excess, *Cell Chem. Biol.*, 2017, **24**(10), 1228–1237, DOI: **10.1016/j.chembiol.2017.08.005**.

90 Y. Lai, F. F. Gao, R. T. Ge, R. Liu, S. Ma and X. Liu, Metal Ions Overloading and Cell Death, *Cell Biol. Toxicol.*, 2024, **40**(1), 72, DOI: **10.1007/s10565-024-09910-4**.

91 H. Öhrvik, Y. Nose, L. K. Wood, B.-E. Kim, S.-C. Gleber, M. Ralle and D. J. Thiele, Ctr2 Regulates Biogenesis of a Cleaved Form of Mammalian Ctr1 Metal Transporter Lacking the Copper- and Cisplatin-Binding Ecto-Domain, *Proc. Natl. Acad. Sci. U. S. A.*, 2013, **110**(46), E4279–E4288, DOI: **10.1073/pnas.1311749110**.

92 A. Espinoza, S. Le Blanc, M. Olivares, F. Pizarro, M. Ruz and M. Arredondo, Iron, Copper, and Zinc Transport: Inhibition of Divalent Metal Transporter 1 (DMT1) and Human Copper Transporter 1 (hCTR1) by shRNA, *Biol. Trace Elem. Res.*, 2012, **146**(2), 281–286, DOI: **10.1007/s12011-011-9243-2**.

93 E. Falcone, B. Vileno, M. Hoang, L. Raibaut and P. Faller, A Luminescent ATCUN Peptide Variant with Enhanced Properties for Copper(II) Sensing in Biological Media, *J. Inorg. Biochem.*, 2021, **221**, 111478, DOI: **10.1016/j.jinorgbio.2021.111478**.

